# Intraband polarization as the source of degenerate four-wave mixing signals in asymmetric semiconductor quantum well structures

Marc Dignam*

*Department of Physics, Queen's University, Kingston, Ontario, Canada, K7L 3N6*

M. Hawton[†]

*Department of Physics, Lakehead University, Thunder Bay, Ontario, Canada, P7B 5E1*

We have developed a formalism for calculating the coherent response of asymmetric semiconductor quantum well structures to ultrashort optical pulses. We work in an excitonic basis and include exciton-exciton interactions via the long-wavelength portion of the excitonic intraband polarization. We apply this formalism to the calculation of degenerate four-wave mixing intensities of a biased semiconductor superlattice and find that many aspects of the four-wave mixing signals are most naturally interpreted as directly resulting from the scattering of excitons off of the intraband polarization grating. We furthermore develop an extremely accurate method of factoring the dynamical equations that does not suffer from the problem encountered by the semiconductor Bloch equations in the Hartree-Fock approximation.

## I. INTRODUCTION

There has been considerable interest over the past 15 years or so in the stationary states and dynamics of electrons and holes in biased semiconductor superlattices (BSSL's), coupled double quantum wells (CDQW's), and other asymmetric quantum well structures (AQWS's). This interest has been generated both by the ability to investigate fundamental questions of semiconductor physics in systems in which the configuration can be specifically tailored, and by the possibility of developing new semiconductor devices. Initially both the experimental and theoretical interest centered on the existence and nature of the stationary states in these systems. More recently work has been focused on the coherent dynamics of the optically generated carriers. The *intraband* dynamics have been examined through the direct detection of the THz field generated by the oscillating electronic wave packets created via short-pulse excitation, while *interband* dynamics have been investigated through pump-probe experiments and time-integrated, time-resolved, and spectrally resolved degenerate four-wave mixing (DFWM) experiments. Although it is generally recognized that there is necessarily a strong connection between the intraband and interband polarization dynamics in these systems, the precise nature of this relationship is not always apparent in the theoretical formalisms used to date to treat them. In this work we show that in AQWS's, the intraband polarization is the dominant source of the DFWM and pump-probe signals.

The most common approaches that have been used in the past to treat the dynamics of electrons and holes near the semiconductor bandedge are the semiconductor Bloch equations (SBE's),[1–4] and various forms of the dynamics controlled truncation (DCT) theory.[5–8] The SBE's have been used successfully to describe a wide range of experimental results, including the ac Stark effect and Rabi oscillations.[2,9] They have the advantage that when used in the Hartree-Fock (HF) approximation, they are in principle non-perturbative in the optical field. In has been shown, however, that the SBE's

within the HF approximation neglect the crucial electron-hole correlations within an exciton when carried out beyond first order in the optical electric field.[6,10–15] The DCT theory on the other hand can in principle treat all correlations exactly to any desired order in the optical field. However, one key difficulty that arises in a DCT calculation is the treatment of the exciton-exciton (XX) Coulomb interaction. A realistic evaluation of the Coulomb matrix elements is extremely computationally intensive. As a result, most DCT calculations employ some sort of simplification. The most common simplifications are to treat the system in a quasi-1D approximation,[7,8,10–12,16,17] to employ a contact or on-site potential for the Coulomb interaction between carriers,[6,18] or to introduce effective interaction parameters.[15] This makes it computationally feasible to include additional features in the model such as disorder[16,19] and electron-phonon interactions.[18] Thus, DCT has been successfully employed to calculate the interband polarization up to fifth order in the optical field in bulk semiconductors and single quantum wells.[12,20] It has also been employed to calculate the intraband polarization of CDQW's and BSSL's to second order.[14,18] However, to our knowledge, DCT has never been used to calculate the third order interband polarization in such complicated ASQW's with or without simplifying the Coulomb interaction.

There have been a large number of papers demonstrating that the inclusion of carrier-carrier correlations are important in the calculation of DFWM signals in bulk semiconductors and quantum wells.[7,8,10–12,15–17] In these papers it is shown that SBE's in the HF approximation lead to errors even to second order in the optical field. One of the key features missing from the Hartree-Fock approximation is the correlation between the electron and hole within a single exciton. This correlation is missing essentially because these equations employ a free electron-hole basis to perform the calculation. Hence when the HF factoring is performed, the correlations between the electron and hole inside the exciton are not treated correctly. This intraexcitonic correlation is auto-

matically incorporated into any theory that employs an excitonic basis.

The excitonic basis has been employed by a number of authors[14,18,21,22] In particular, it has been used to investigate the intraband dynamics of CDQW's (Ref. 18) and BSSL's (Ref. 14) to second order. To treat interactions to third order and beyond requires the evaluation of exciton-exciton interactions. This has been done in the excitonic basis for a single quantum well in a magnetic field.[21] However, the treatment of more complicated systems such as an AQWS to third order can become very computationally intensive if one does not find an efficient way of dealing with the exciton-exciton interactions. It is with this aim in mind that this work has been performed.

In this paper we present a new formalism for the calculation of DFWM and pump-probe signals in AQWS's. The two key features of our approach are that (1) it employs an excitonic basis that includes the center-of-mass (c.m.) wave vector of the excitons and (2) it expresses the interexcitonic interaction in terms of the intraband polarization in the long-wavelength limit $\mathbf{P}_<^{intra}$. As discussed above, the advantage of the excitonic basis is that it ensures that electron-hole correlations within an exciton are treated correctly. Furthermore, keeping track of the c.m. wave vectors of the excitons allows us to determine which terms in our dynamical equation contribute to radiation in a given direction.

We base our excitonic theory on the quasi-Bosonic treatment of Hawton and Nelson[23] that has been used successfully in the calculation of the second-order intraband polarization of a BSSL.[14] The treatment of the interexcitonic interaction via $\mathbf{P}_<^{intra}$ neglects XX correlations and treats XX interactions in the dipole approximation. In a system *with* inversion symmetry, such as a bulk semiconductor, the interexcitonic interaction would be zero in the dipole approximation ($\mathbf{P}_<^{intra}=0$), and the interaction would then be governed entirely by XX correlations[7,10–12,15–17] and perhaps biexcitonic effects.[20,24] However, in AQWS's, due to the broken symmetry of the system, a large macroscopic intraband polarization $\mathbf{P}_<^{intra}$ generally arises. The contribution of $\mathbf{P}_<^{intra}$ to the interexcitonic interactions is thus dominant over any short-range interexcitonic Coulomb effects arising from XX correlations. It is therefore a very good approximation to neglect the XX correlations in AQWS's, as we do in this work.

The XX interaction is incorporated in the Hamiltonian by expressing the long-wavelength portion of the Coulomb interaction as a spatial integral over $\mathbf{P}_<^{intra} \cdot \mathbf{P}_<^{intra}$. The Hamiltonian is written in an excitonic basis and used to obtain the equations of motion for exciton correlation functions that are then used to calculate the DFWM signal to third order in the optical field. This result is obtained in the spirit of DCT without factorization. We show, however, that a factorization at the level of the XX interactions is possible that yields almost identical results to the unfactored equations.

To provide a concrete system with which to demonstrate our approach we calculate the DFWM signals from a BSSL. This is an interesting system in part because of the long history of investigations into the electron states and dynamics in periodic structures in dc electric fields, and in part due to the clear signatures of interband and intraband dynamics in these systems. The electronic stationary states in a periodic potential with period $d$ in the presence of an external dc electric field $E_{dc}$ are localized in a one-band approximation and have energies $E_n = E_0 + enE_{dc}d$, where $n$ is an integer.[25] These equally spaced states form the so-called Wannier Stark ladder (WSL) in the BSSL; they were first evidenced experimentally by Mendez *et al.*,[26] and have been theoretically treated with the inclusion of excitonic effects by a number of authors.[27–30]

Shortly after the experimental observation of the WSL states, the dynamical behavior of excitons in BSSL's were investigated both theoretically[31] and experimentally.[32–38] It has long been predicted[39] that the centroid of electronic wave packets in a periodic potential with an external electric field will undergo periodic oscillations with a frequency $\omega_B = edE_{dc}/\hbar$. These are the well known Bloch oscillations (BO's), where $\omega_B$ is the BO frequency. Experimentally, Bloch-oscillating electronic wave packets can be created in an undoped BSSL by using an ultrashort ($\sim 100$ fs) across-bandgap optical pulse. This results in the creation of a Bloch-oscillating electron-hole wave packet that is a coherent superposition of excitonic WSL states.[31–33] The evidence for Bloch-oscillating wave packets has been obtained either through time-integrated degenerate four-wave mixing (DFWM) signals,[32,33,38] the direct detection of the THz field generated by the oscillating excitonic intraband dipole,[34] or through oscillations of the excitonic peaks in spectrally resolved DFWM experiments.[35–37]

To date, there have been few calculations of DFWM signals for biased superlattices. Some of the earliest calculations of DFWM signals in a BSSL were done by Von Plessen and Thomas.[40] This work presented the first prediction that the signature of BO would appear in the DFWM signals. These calculations were performed on the basis of noninteracting electrons and holes; they thus ignored excitonic effects, which are very important in these systems as it is excitons that are predominantly created. Some later theories have included excitonic effects in a phenomenological way by treating the BSSL as a sort of generic multilevel system.[33] The BSSL has also been modeled using the SBE's in the HF approximation.[41–44] As discussed above, such calculations neglect the intraexcitonic electron-hole correlations, which have been shown to be very important in this system.[6,45] Our work is the first calculation of the DFWM signals in a BSSL that includes both the intraexcitonic electron-hole correlation along with the XX interaction. We find that the DFWM signals are most naturally seen as the result of excitons scattering off of the grating created by the intraband polarization.

The paper is organized as follows. In Sec. II we write the Hamiltonian in terms of exciton annihilation and creation operators, external fields and excitonic polarization. In Sec. III we derive the equations of motion for the exciton operators in the Heisenberg picture. We use these to obtain a system of equations for the phenomenologically damped correlation functions that give the DFWM and pump-probe signals to third order. In Sec. IV we present a factored version of the equations. In Sec. V we present the results of

numerical calculations of intraband polarization and time-resolved and time-integrated DFWM signals for a BSSL. We present our conclusions in Sec. VI.

## II. THE EXCITON HAMILTONIAN

In this section we obtain a Hamiltonian describing excitons in an AQWS in the presence of optical and THz electric fields. We include explicitly in our Hamiltonian only the electrons in the highest energy valence band (VB) miniband and the lowest energy conduction band (CB) miniband. From here on we call these the system electrons. We treat the electric field effects of any charges (ions and electrons) that are not included in $U^{\text{ext}}(\mathbf{r})$ by introducing an effective static dielectric constant $\varepsilon$ in the usual way. Thus we take the ac electric field (optical plus THz) seen by the system electrons $\mathbf{E} = \mathbf{D}/\varepsilon$, to arise from externally applied fields as modified by $\varepsilon = \varepsilon_0(1+\chi)$ where $\chi$ is the electric susceptibility of the background charges. Using the usual dipole approximation for the interaction of the system electrons with $\mathbf{E}$, the Hamiltonian can be written in the form

$$H = \sum_{\alpha} \left[ \frac{\mathbf{p}_{\alpha}^2}{2m_e} + U^{\text{ext}}(\mathbf{r}_{\alpha}) \right] + V_{\text{coul}} - \int d^3\mathbf{r} \, \mathbf{E}(\mathbf{r},t) \cdot \mathbf{P}^{\text{ex}}(\mathbf{r},t),$$
(2.1)

where

$$V_{\text{coul}} = \sum_{\alpha} V_{\alpha}^{\text{self}} + \sum_{\alpha \neq \beta} \frac{e^2}{8\pi\varepsilon|\mathbf{r}_{\alpha} - \mathbf{r}_{\beta}|}$$
(2.2)

is the screened Coulomb energy, including the self-energy $V_{\alpha}^{\text{self}}$ of each of the system electrons and $\mathbf{P}^{\text{ex}}$ is the polarization due to the system electrons (excitons). The subscript $\alpha$ labels the system electron with momentum $\mathbf{p}_{\alpha}$ and position $\mathbf{r}_{\alpha}$. The mass of the electron is $m_e$ and its charge is $-e$. The applied ac field is the sum of a THz field and an optical field

$$\mathbf{E}(\mathbf{r},t) = \mathbf{E}^{\text{THz}}(\mathbf{r},t) + \mathbf{E}^{\text{opt}}(\mathbf{r},t).$$
(2.3)

In what follows, the time dependence in the electric field and polarization is implicit and will not usually be explicitly included. The screened Coulomb energy can be written as[46]

$$V_{\text{coul}} = \frac{\varepsilon}{2} \int d^3\mathbf{r} \, E_{\|}^2(\mathbf{r}),$$
(2.4)

where $E_{\|}(\mathbf{r})$ is the longitudinal component of the electric field arising from the system electrons. The electric field satisfies $\mathbf{D} = \varepsilon\mathbf{E} + \mathbf{P}^{\text{ex}}$. Since the system is globally neutral, the longitudinal part of the displacement field is zero, and it thus follows that $\mathbf{P}_{\|}^{\text{ex}}(\mathbf{r}) = -\varepsilon\mathbf{E}_{\|}(\mathbf{r})$, where $\mathbf{P}_{\|}^{\text{ex}}(\mathbf{r})$ is the longitudinal portion of the exciton polarization. Using this result, we obtain

$$V_{\text{coul}} = \frac{1}{2\varepsilon} \int d^3\mathbf{r} \, \mathbf{P}_{\|}^{\text{ex}}(\mathbf{r}) \cdot \mathbf{P}_{\|}^{\text{ex}}(\mathbf{r}) = \frac{1}{2\varepsilon} \int d^3\mathbf{k} \, |\mathcal{P}_{\|}^{\text{ex}}(\mathbf{k})|^2,$$
(2.5)

where $\mathcal{P}_{\|}^{\text{ex}}(\mathbf{k})$ is the Fourier transform of $\mathbf{P}_{\|}^{\text{ex}}(\mathbf{r})$.

Calculating $\mathbf{P}_{\|}^{\text{ex}}(\mathbf{r})$ exactly is clearly an extremely demanding task; instead, we look for a suitable approximation. There are two key pieces that we need to include in the expression for $V_{\text{coul}}$. First, it must accurately contain the Coulomb interaction between an electron and hole within a single exciton. Second, it must include the major contribution to the interaction between excitons. For the DFWM experiments considered in this work, the optical field that creates the excitons consists of two pulses with central angular frequencies $\omega_c$, amplitudes $\mathbf{E}_i$, and wave vectors $\mathbf{K}_i$ for $i = \{1,2\}$. Because we wish to calculate the generated THz radiation and DFWM signals, we are interested in the portion of the polarization created by these optical pulses that varies on length scales on the order of the optical wavelength or larger. The wavelengths of these modes are thus large relative to the size of the bound excitons, which is given roughly by the exciton Bohr radius $a_0$.

For the experiments that we are interested in modelling, the exciton-exciton correlations (e.g., biexcitonic effects) are not considered to be particularly important. We thus treat the Coulomb interaction between carriers in the long-wavelength limit as follows. We break the integral over $\mathbf{k}$ in Eq. (2.5) into an integral near the origin of $\mathbf{k}$ space (long-wavelength portion) and an integral over the rest of the space. Thus

$$V_{\text{coul}} = V_{\text{long}} + V_{\text{short}}.$$
(2.6)

We then form electron-hole pairs labeled by $\gamma$ and extract from $V_{\text{coul}}$ the pieces which contain the interaction between the electron and hole within each pair. As is shown in Appendix A, only $V_{\text{short}}$ contributes to the electron-hole interaction within each exciton. The remaining portion of the Coulomb interaction $V_{\text{long}}$ can be written simply as

$$V_{\text{long}} = \frac{1}{2\varepsilon} \int d^3\mathbf{R} \, \mathbf{P}_{<,\|}^{\text{ex}}(\mathbf{R}) \cdot \mathbf{P}_{<,\|}^{\text{ex}}(\mathbf{R}),$$
(2.7)

where $\mathbf{P}_{<,\|}^{\text{ex}}(\mathbf{R})$ is the longitudinal part of the excitonic polarization in the long-wavelength approximation. The Hamiltonian thus becomes

$$H = \sum_{\gamma} H_{\gamma}^{\text{ex}} - \int d^3\mathbf{R} \, \mathbf{E}(\mathbf{R}) \cdot \mathbf{P}^{\text{ex}}(\mathbf{R})$$

$$+ \frac{1}{2\varepsilon} \int d^3\mathbf{R} \, \mathbf{P}_{<,\|}^{\text{ex}}(\mathbf{R}) \cdot \mathbf{P}_{<,\|}^{\text{ex}}(\mathbf{R}),$$
(2.8)

where $H_{\gamma}^{\text{ex}}$ is defined by

$$\sum_{\gamma} [H_{\gamma}^{\text{ex}} - V_{\text{short}}] \equiv \sum_{\alpha} \left[ \frac{\mathbf{p}_{\alpha}^2}{2m_e} + U^{\text{ext}}(\mathbf{r}_{\alpha}) \right].$$

As is discussed at the end of Appendix A, we can safely replace $V_{\text{short}}$ in the definition of $H_{\gamma}^{\text{ex}}$ by the full $V_{\text{coul}}$ as long as the system is large compared to the exciton Bohr radius; thus, $H_{\gamma}^{\text{ex}}$ is indeed the usual single-exciton Hamiltonian. We show in Appendix A that in the long-wavelength limit, the spatial dependence in the polarization arises from the center-of-mass spatial position of the excitons. Therefore, the integration variable $\mathbf{R}$ in Eq. (2.8) is simply the exciton center of mass position.

The excitonic polarization can be written as the sum of interband and intraband polarizations (see Appendix B). The

longitudinal polarization in Eq. (2.8) contains both the inter-band polarization $\mathbf{P}_<^{\text{inter}}(\mathbf{R})$, and intraband polarization $\mathbf{P}_<^{\text{intra}}(\mathbf{R})$ contributions. However, as is shown in Appendix A, the interband contribution to this polarization is generally negligible. In addition, because in practice the extent of the AQWS in the $z$ direction is much less than the spatial period of the intraband polarization, we can replace $\mathbf{P}_{<\parallel}^{\text{ex}}(\mathbf{R})$ in the last term in the Hamiltonian by the full intraband polarization arising from the excitons. Thus, the Hamiltonian becomes

$$H = \sum_\gamma H_\gamma^{\text{ex}} - \int d^3\mathbf{R}\; \mathbf{E}(\mathbf{R}) \cdot \mathbf{P}_<(\mathbf{R})$$
$$+ \frac{1}{2\varepsilon} \int d^3\mathbf{R}\; \mathbf{P}_<^{\text{intra}}(\mathbf{R}) \cdot \mathbf{P}_<^{\text{intra}}(\mathbf{R}), \qquad (2.9)$$

where $\mathbf{P}_<(\mathbf{R}) = \mathbf{P}_<^{\text{inter}}(\mathbf{R}) + \mathbf{P}_<^{\text{intra}}(\mathbf{R})$. Note that $\mathbf{E}(\mathbf{R})$ in the above Hamiltonian does not include any static external bias fields, as these have been incorporated into the potential energy in $H_\gamma^{\text{ex}}$. The third term in Eq. (2.9) contains the XX Coulomb interactions in the long-wavelength limit.

We now wish to write the Hamiltonian in second-quantized form. As in earlier work,[14] we employ a basis of excitonic states in the presence of the external dc electric field $E_{\text{dc}}$. The envelope functions for these states can be written in the form

$$\Psi_{\mu,\mathbf{K}}(\mathbf{r}_e; \mathbf{r}_h) = \frac{e^{i\mathbf{K}_\parallel \cdot \mathbf{R}_\parallel}}{\sqrt{A}} \chi_{\mu,K_z}(\mathbf{r}_\parallel; Z, z), \qquad (2.10)$$

where $\mu$ represents the quantum numbers of internal motion, $\mathbf{K} = (\mathbf{K}_\parallel, K_z)$ is the center of mass wave vector, $\mathbf{r} = (\mathbf{r}_\parallel, z)$ is the electron-hole separation, $\mathbf{R} = (\mathbf{R}_\parallel, Z)$ is the position of the center of mass of the exciton, $A$ is the transverse area of the structure, and $\chi_{\mu,K_z}(\mathbf{r}_\parallel; Z, z)$ is the usual envelope function for the internal motion and center-of-mass motion in the $z$ direction.[27] In this basis, the noninteracting exciton Hamiltonian in second-quantized form can be written as

$$H_0^{\text{ex}} \equiv \sum_{\mu,\mathbf{K}} \hbar\omega_\mu^{\mathbf{K}} B_{\mu,\mathbf{K}}^\dagger B_{\mu,\mathbf{K}}, \qquad (2.11)$$

where $B_{\mu,\mathbf{K}}^\dagger$ is the creation operator for a exciton with center of mass wave vector $\mathbf{K}$, internal quantum numbers $\mu$ and energy $\hbar\omega_\mu^{\mathbf{K}}$. Because the optical photon momenta are so small, the wave vectors of the optically excited excitons will also be small. Thus in the following, we shall employ the approximation $\omega_\mu^{\mathbf{K}} \simeq \omega_\mu^{\mathbf{K}=0} \equiv \omega_\mu$. The only way to generate larger momentum excitons is through scattering, and since these will not contribute directly to the polarization, we neglect them in this work.

For the two-pulse DFWM experiments that we are modelling, the incident optical fields of pulse 1 and pulse 2 have definite wave vectors $\mathbf{K}_1$ and $\mathbf{K}_2$ respectively. Furthermore, we consider applied THz fields that also have a definite wave vector. Thus, the total applied ac field can be written as discrete Fourier series in the form

$$\mathbf{E}(\mathbf{R}) = \sum_\mathbf{K} \mathbf{E}_\mathbf{K} e^{i\mathbf{K}\cdot\mathbf{R}}. \qquad (2.12)$$

In the long-wavelength limit, therefore, the polarization can also be written as a discrete Fourier series that will contain wave-vectors such as $\mathbf{K}_1$, $\mathbf{K}_2$, and $2\mathbf{K}_2 - \mathbf{K}_1$, etc. Thus we write

$$\mathbf{P}_<(\mathbf{R}) = \sum_\mathbf{K}^{K<K_M} e^{i\mathbf{K}\cdot\mathbf{R}} \mathbf{P}_\mathbf{K}, \qquad (2.13)$$

where

$$\mathbf{P}_\mathbf{K} = \mathbf{P}_\mathbf{K}^{\text{inter}} + \mathbf{P}_\mathbf{K}^{\text{intra}}, \qquad (2.14)$$

$\mathbf{P}_\mathbf{K}^{\text{inter}}$ and $\mathbf{P}_\mathbf{K}^{\text{intra}}$ are the $\mathbf{K}$th Fourier components of the interband and intraband polarizations, respectively, and the sum is only over small wave vectors $|\mathbf{K}| < |\mathbf{K}_M|$ for $|\mathbf{K}_M| \ll 2\pi/a_0$. As is shown in Appendix B, the intraband component in the usual dipole approximation is given by

$$\mathbf{P}_\mathbf{K}^{\text{inter}} = \frac{1}{V} \sum_\mu [\mathbf{M}_\mu B_{\mu,-\mathbf{K}}^\dagger + \mathbf{M}_\mu^* B_{\mu,\mathbf{K}}], \qquad (2.15)$$

where

$$\mathbf{M}_\mu = \mathbf{M}_0 \sqrt{A} \int dZ \chi_{\mu,0}^*(\mathbf{r}_\parallel = 0; Z, z = 0) \qquad (2.16)$$

is the interband dipole matrix element, with $\mathbf{M}^0$ being the bulk interband dipole matrix element. The intraband component of the polarization again in the dipole approximation is given by

$$\mathbf{P}_\mathbf{K}^{\text{intra}} = \frac{1}{V} \sum_{\mathbf{K}'} \sum_{\mu,\mu'} \mathbf{G}_{\mu,\mu'} B_{\mu,\mathbf{K}'}^\dagger B_{\mu',\mathbf{K}+\mathbf{K}'}, \qquad (2.17)$$

where

$$\mathbf{G}_{\mu,\mu'} \equiv -e \int_V d^3\mathbf{r}_e \int_V d^3\mathbf{r}_h \Psi_{\mu,0}^*(\mathbf{r}_e; \mathbf{r}_h)(\mathbf{r}_e - \mathbf{r}_h)\Psi_{\mu',0}(\mathbf{r}_e; \mathbf{r}_h)$$
$$(2.18)$$

is the intraband dipole matrix element between two excitonic states. Equations (2.15)–(2.17) are general. However, as is discussed in Appendix B, Eq. (2.18) is only valid for bound excitons. The more general expression for bound and unbound excitons is given in Appendix B.

The Hamiltonian is thus finally given simply by

$$H = H_0^{\text{ex}} + V \sum_\mathbf{K}^{K<K_M} \left( -\mathbf{E}_{-\mathbf{K}} \cdot \mathbf{P}_\mathbf{K} + \frac{1}{2\varepsilon} \mathbf{P}_{-\mathbf{K}}^{\text{intra}} \cdot \mathbf{P}_\mathbf{K}^{\text{intra}} \right). \qquad (2.19)$$

One key feature of this Hamiltonian is its dependence on on $\mathbf{K}$. This is important if one is to calculate the nonlinear intensity propagating in a particular direction; for example, the

electric field of the DFWM signal propagating in the $2\mathbf{K}_2 - \mathbf{K}_1$ direction is proportional to $\mathbf{P}^{\mathrm{inter}}_{2\mathbf{K}_2-\mathbf{K}_1}$. Thus, it is essential that we keep track of the different Fourier components of the polarization in our calculation. This is analogous to the spatial Fourier expansion approach employed by previous authors[47] when employing the SBE's. Without keeping track of the exciton c.m. momenta, we find that there arises an ambiguity as to which terms should be kept when expanding to a given order in the optical field (see Sec. III).

We stress that the Hamiltonian as derived above is general and may be applied to any AQWS. For infinite superlattices or multiple quantum well structures, the c.m. wave vector $\mathbf{K}$ is three dimensional. However, for a finite superlattice or nonperiodic AQWS, $\mathbf{K}$ is restricted to the plane perpendicular to the growth axis ($x$-$y$ plane) and the internal quantum number $\mu$ is taken to include the c.m. motion of the excitons in the $z$ direction.

### III. EXCITON DYNAMICS

Now that we have the Hamiltonian for the system of interacting excitons in external optical and THz fields, we can determine the dynamics by: finding the excitonic stationary states and energy levels, calculating the equations of motion for the relevant correlation functions, and then calculating the time dependence of the nonlinear polarization. We assume that the excitonic states have been calculated and now proceed with determining the dynamical equations.

Using the Hamiltonian given by Eq. (2.19), the equations of motion $i\hbar \, dB^{\dagger}_{\mu,\mathbf{K}}/dt = [B^{\dagger}_{\mu,\mathbf{K}}, H]$ become

$$i\hbar \frac{dB^{\dagger}_{\mu,\mathbf{K}}}{dt} = [B^{\dagger}_{\mu,\mathbf{K}}, H^{\mathrm{ex}}_0] - V \sum_{\mathbf{K}'} \mathbf{E}_{-\mathbf{K}'} \cdot [B^{\dagger}_{\mu,\mathbf{K}}, \mathbf{P}_{\mathbf{K}'}]$$

$$+ \frac{V}{2\varepsilon} \sum_{\mathbf{K}'} \{ \mathbf{P}^{\mathrm{intra}}_{-\mathbf{K}'} \cdot [B^{\dagger}_{\mu,\mathbf{K}}, \mathbf{P}^{\mathrm{intra}}_{\mathbf{K}'}]$$

$$+ [B^{\dagger}_{\mu,\mathbf{K}}, \mathbf{P}^{\mathrm{intra}}_{\mathbf{K}'}] \cdot \mathbf{P}^{\mathrm{intra}}_{-\mathbf{K}'} \}. \quad (3.1)$$

After substitution of Eqs. (2.15) and (2.17), the second commutator in Eq. (3.1) becomes

$$[B^{\dagger}_{\mu,\mathbf{K}}, \mathbf{P}_{\mathbf{K}'}] = \frac{1}{V} \sum_{\mu'} \mathbf{M}^*_{\mu'} [B^{\dagger}_{\mu,\mathbf{K}}, B_{\mu',\mathbf{K}'}]$$

$$+ \frac{1}{V} \sum_{\mu',\mu'',\mathbf{K}''} \mathbf{G}_{\mu',\mu''} B^{\dagger}_{\mu',\mathbf{K}''} [B^{\dagger}_{\mu,\mathbf{K}}, B_{\mu'',\mathbf{K}''+\mathbf{K}'}].$$

$$(3.2)$$

As has been shown by Hawton and Nelson,[23] the commutators for the excitonic operators take the form

$$[B_{\mu,\mathbf{K}}, B^{\dagger}_{\mu',\mathbf{K}'}] = \delta_{\mu,\mu'} \delta_{\mathbf{K},\mathbf{K}'}$$

$$- 2 \sum_{\mu'',\mu'''} X^{\mu,\mu';\mathbf{K},\mathbf{K}'}_{\mu'',\mu'''} B^{\dagger}_{\mu''',\mathbf{K}'} B_{\mu'',\mathbf{K}}. \quad (3.3)$$

The second term in Eq. (3.3) is simply the effect of phase-space filling (PSF) and quantifies the degree to which the excitons deviate from ideal Bosons. Putting the above three equations together and neglecting nonresonant terms in the usual rotating-wave approximation, we obtain

$$i\hbar \frac{dB^{\dagger}_{\mu,\mathbf{K}}}{dt} = -\hbar \omega_\mu B^{\dagger}_{\mu,\mathbf{K}} + \mathbf{E}^{\mathrm{opt}}_{-\mathbf{K}} \cdot \mathbf{M}^*_\mu + \sum_{\mu',\mathbf{K}'} \mathbf{E}^{\mathrm{THz}}_{-\mathbf{K}'} \cdot \mathbf{G}_{\mu',\mu} B^{\dagger}_{\mu',\mathbf{K}-\mathbf{K}'} + 2 \sum_{\mu',\mu'',\mu''',\mathbf{K}'} \hbar \omega_{\mu'} X^{\mu',\mu;\mathbf{K}',\mathbf{K}}_{\mu'',\mu'''} B^{\dagger}_{\mu',\mathbf{K}'} B^{\dagger}_{\mu''',\mathbf{K}} B_{\mu'',\mathbf{K}'}$$

$$- 2 \sum_{\mu',\mu'',\mu''',\mathbf{K}'} \mathbf{E}^{\mathrm{opt}}_{-\mathbf{K}'} \cdot \mathbf{M}^*_{\mu'} X^{\mu';\mu;\mathbf{K}',\mathbf{K}}_{\mu'';\mu'''} B^{\dagger}_{\mu''',\mathbf{K}} B_{\mu'',\mathbf{K}'} - 2 \sum_{\mu',\mu'',\mu''',\mu'''',\mathbf{K}',\mathbf{K}''} \mathbf{E}^{\mathrm{THz}}_{-\mathbf{K}'} \cdot \mathbf{G}_{\mu',\mu''} X^{\mu'',\mu;\mathbf{K}'+\mathbf{K}'',\mathbf{K}}_{\mu''',\mu'''} B^{\dagger}_{\mu',\mathbf{K}''}$$

$$\times B^{\dagger}_{\mu''',\mathbf{K}} B_{\mu''',\mathbf{K}'+\mathbf{K}''} - \frac{1}{\varepsilon V} \sum_{\mu',\mu'',\mu'''',\mathbf{K}',\mathbf{K}''} \mathbf{G}_{\mu',\mu''} \cdot \mathbf{G}_{\mu'''',\mu} \mathcal{S}\{B^{\dagger}_{\mu'''',\mathbf{K}-\mathbf{K}'}; B^{\dagger}_{\mu',\mathbf{K}''} B_{\mu'',-\mathbf{K}'+\mathbf{K}''}\}$$

$$+ \frac{2}{\varepsilon V} \sum_{\mathbf{K}',\mathbf{K}'',\mathbf{K}'''} \sum_{\mu',\mu'',\mu''''} \sum_{\mu''',\mu''',\mu''''} \mathbf{G}_{\mu',\mu''} \cdot \mathbf{G}_{\mu'''',\mu''''} X^{\mu'''',\mu;\mathbf{K}'+\mathbf{K}''',\mathbf{K}}_{\mu''',\mu'''} \mathcal{S}\{B^{\dagger}_{\mu',\mathbf{K}''} B_{\mu'',-\mathbf{K}'+\mathbf{K}''}; B^{\dagger}_{\mu'''',\mathbf{K}'''} B^{\dagger}_{\mu''',\mathbf{K}} B_{\mu''',\mathbf{K}'+\mathbf{K}'''}\},$$

$$(3.4)$$

where $\mathcal{S}\{A;B\} \equiv \frac{1}{2}\{AB + BA\}$ is a symmetrizer. In fact, one can show that in the limit of a large system ($V \to \infty$), the symmetrization is unnecessary, as the extra terms that are added all go to zero as $V \to \infty$. As a result of this, it is easy to

see that the order of the exciton operators in the above expression is of no consequence and the symmetrizers can be ignored.

We stress that the treatment of the XX interaction in the

long-wavelength limit is very different than the HF approximation employed in the SBE approach. In the language employed by many authors,[7,8,10–12,15–17] the HF approximation includes only first order Coulomb effects, and misses out higher correlations. In those works, it is often found that the higher correlations largely cancel out the effects of the first order Coulomb terms. The same separation of Coulomb effects is not exhibited within our formalism, as we explicitly include electron-hole correlations within excitons and only neglect small-wavelength XX correlations. Thus, our approach includes many of the higher-order correlations discussed in work by previous authors.

We now use the above dynamic equation to obtain the expressions for the interband and intraband correlation functions up to third order in the optical field. The time derivatives of the operator products can be obtained by simply using the product rule of differential calculus and Eq. (3.4). To obtain the expectation values, we employ phenomenological damping to account for processes such as carrier-carrier scattering, electron-phonon interactions, impurities, and defects. We consider now the case where there are two optical pulses with central frequency $\omega_c$ and with wave vectors $\mathbf{K}_1$ and $\mathbf{K}_2$ incident on the superlattice. Thus, the total external optical field is given by

$$\mathbf{E}^{\mathrm{opt}}(\mathbf{R},t) = \mathbf{E}_1(t) e^{i(\mathbf{K}_1 \cdot \mathbf{R} - \omega_c t)} + \mathbf{E}_2(t) e^{i(\mathbf{K}_2 \cdot \mathbf{R} - \omega_c t)} + \mathrm{c.c.}, \tag{3.5}$$

so that we have

$$\mathbf{E}_{-\mathbf{K}_j}^{\mathrm{opt}}(t) = \mathbf{E}_j^*(t) e^{i\omega_c t}. \tag{3.6}$$

We consider a THz field with a single wave vector $\mathbf{K}_T$. Now, $|\mathbf{K}_T| \ll |\mathbf{K}_1|, |\mathbf{K}_2|$ and there is a spread in the wave vectors of the optical pulses associated with the finite dimensions of the beams. Thus, $|\mathbf{K}_T|$ is much less than the standard deviations of the optical pulses and so we neglect $\mathbf{K}_T$ in the remainder of the paper and set

$$\mathbf{E}_{\mathbf{K}}^{\mathrm{THz}}(t) = \delta_{\mathbf{K},0} \mathbf{E}^{\mathrm{THz}}(t). \tag{3.7}$$

Using these expressions for the external ac fields, we obtain the equations of motion for the correlation functions up to third order in the optical field. The matrix that quantifies PSF is given by[23]

$$X_{\mu'',\mu'''}^{\mu,\mu';\mathbf{K},\mathbf{K}'} \approx X_{\mu'',\mu'''}^{\mu,\mu';0,0} = \sum_{\mathbf{k}} \psi_{\mathbf{k}}^{\mu,0*} \psi_{\mathbf{k}}^{\mu',0} \psi_{\mathbf{k}}^{\mu'',0*} \psi_{\mathbf{k}}^{\mu''',0}. \tag{3.8}$$

Because the momenta of the optically created excitons are small, and the dependence of $X_{\mu'',\mu'''}^{\mu,\mu';\mathbf{K},\mathbf{K}}$ on $\mathbf{K}$ and $\mathbf{K}'$ is very weak, we have neglected the $\mathbf{K}$ dependence in the final expression. To simplify notation, we shall denote $X_{\mu'',\mu'''}^{\mu,\mu'} = X_{\mu'',\mu'''}^{\mu,\mu';0,0}$ from now on. In the above expression for $X_{\mu'',\mu'''}^{\mu,\mu';0,0}$, the $\psi_{\mathbf{k}}^{\mu,\mathbf{K}}$ are the expansion coefficients of the exciton envelope function, $\Psi_{\mu,\mathbf{K}}(\mathbf{r}_e; \mathbf{r}_h)$, in the free electron-hole basis, as described in Appendix B.

From the above results, we can easily derive the equations of motion for the correlation functions required to calculate the DFWM signal in the $2\mathbf{K}_2 - \mathbf{K}_1$ direction. Neglecting propagation effects within the structure in the usual way, the DFWM optical *field* in the $2\mathbf{K}_2 - \mathbf{K}_1$ direction to third order is simply proportional to $\mathbf{P}_{2\mathbf{K}_2 - \mathbf{K}_1}^{\mathrm{inter}(3)}$. Thus the DFWM *intensity* in this direction is proportional to $|(1/V) \Sigma_\mu \mathbf{M}_\mu \langle B_{\mu,2\mathbf{K}_2 - \mathbf{K}_1}^\dagger \rangle^{(3)}|^2$, where the superscript (3) denotes third order in the optical fields. Note that our notation is that the order of a given correlation function is usually simply given by the number of exciton operators in the function. When this is not the case, the order of the function is given as a superscript, as, for example, in the case of $\langle B_{\mu,2\mathbf{K}_2 - \mathbf{K}_1}^\dagger \rangle^{(3)}$. Thus the DFWM signal is determined by the dynamical equation for the creation operator for the excitons moving in the $2\mathbf{K}_2 - \mathbf{K}_1$ direction. From Eq. (3.4), the equation of motion for $\langle B_{\mu,2\mathbf{K}_2 - \mathbf{K}_1}^\dagger \rangle^{(3)}$ is

$$i\hbar \frac{d \langle B_{\mu,2\mathbf{K}_2 - \mathbf{K}_1}^\dagger \rangle^{(3)}}{dt}$$

$$= -\left( \hbar \omega_\mu^0 + \frac{i\hbar}{T_\mu^{(22\bar{1})}} \right) \langle B_{\mu,2\mathbf{K}_2 - \mathbf{K}_1}^\dagger \rangle^{(3)}$$

$$- \frac{1}{\varepsilon V} \sum_{\mu',\mu'',\mu'''} \mathbf{G}_{\mu',\mu''} \cdot \mathbf{G}_{\mu''',\mu} \langle B_{\mu''',\mathbf{K}_2}^\dagger B_{\mu',\mathbf{K}_2}^\dagger B_{\mu'',\mathbf{K}_1} \rangle$$

$$+ \mathbf{E}^{\mathrm{THz}} \cdot \sum_{\mu'} \mathbf{G}_{\mu',\mu} \langle B_{\mu',2\mathbf{K}_2 - \mathbf{K}_1}^\dagger \rangle^{(3)}. \tag{3.9}$$

Equation (3.9) depends explicitly upon the third-order correlation function $\langle B_{\mu''',\mathbf{K}_2}^\dagger B_{\mu',\mathbf{K}_2}^\dagger B_{\mu'',\mathbf{K}_1} \rangle$; the equation of motion of $\langle B_{\mu''',\mathbf{K}_2}^\dagger B_{\mu',\mathbf{K}_2}^\dagger B_{\mu'',\mathbf{K}_1} \rangle$ depends (either explicitly or implicitly) upon the second and first order correlation functions $\langle B_{\mu,\mathbf{K}_2}^\dagger B_{\mu',\mathbf{K}_1} \rangle$, $\langle B_{\mu,\mathbf{K}_2}^\dagger B_{\mu',\mathbf{K}_2}^\dagger \rangle$, $\langle B_{\mu,\mathbf{K}_1}^\dagger \rangle$, and $\langle B_{\mu,\mathbf{K}_2}^\dagger \rangle$. The equations of motion for these correlation functions are easily derived from Eq. (3.4) by using the product rule. The $T_\mu^{(22\bar{1})}$ in Eq. (3.9) are the phenomenological time constants associated with interband dephasing. This and the time constants associated with the other correlations functions are discussed in Sec. V. Note that many of the terms found in Eq. (3.4)—including terms in the sums over $\mathbf{K}'$ and $\mathbf{K}''$—are not found in Eq. (3.9) because they are necessarily higher than third order in the optical field. As we show below, this is not the case for the third-order equations for $\langle B_{\mu,\mathbf{K}}^\dagger \rangle^{(3)}$ for all $\mathbf{K}$.

There are a number of interesting features contained in Eq. (3.9). First, this equation does not contain any PSF terms (either explicitly or implicitly). This arises because PSF does not result in a change in the exciton momentum. As a result PSF does not occur until fifth order for DFWM calculations. It has been noted by previous authors employing the SBE's (Ref. 44) that the PSF is very small in this system. However, here we show that to third order it is rigorously zero. The

ability to determine that PSF does not contribute to the third order DFWM signal is due entirely to the fact that we keep track of the c.m. wave vectors of the excitons.

It is interesting to note that PSF does contribute to the signal in a pump-probe experiment. For example, to third order in the optical fields, the dynamic equation for the correlation function needed to calculate the pump-probe signal in the $\mathbf{K}_2$ direction is

$$
i\hbar \frac{d\langle B_{\mu,\mathbf{K}_2}^\dagger\rangle^{(3)}}{dt} = -\left(\hbar\omega_\mu + \frac{i\hbar}{T_\mu^{(1)}}\right)\langle B_{\mu,\mathbf{K}_2}^\dagger\rangle^{(3)} + \mathbf{E}^{\mathrm{THz}}\cdot\sum_{\mu'}\mathbf{G}_{\mu';\mu}\langle B_{\mu',\mathbf{K}_2}^\dagger\rangle^{(3)} + 2\sum_{\mu',\mu'',\mu''',i=1,2}\hbar\omega_{\mu'}X_{\mu'',\mu'''}^{\mu',\mu}\langle B_{\mu''',\mathbf{K}_2}^\dagger B_{\mu',\mathbf{K}_i}^\dagger B_{\mu'',\mathbf{K}_i}\rangle
$$

$$
-2\sum_{\mu',\mu'',\mu''',i=1,2}\mathbf{E}_i^* e^{i\omega_c t}\cdot\mathbf{M}_{\mu'}^* X_{\mu'',\mu'''}^{\mu',\mu}\langle B_{\mu''',\mathbf{K}_2}^\dagger B_{\mu'',\mathbf{K}_i}\rangle - 2\mathbf{E}^{\mathrm{THz}}\cdot\sum_{\mu',\mu'',\mu''',\mu'''',i=1,2}\mathbf{G}_{\mu',\mu''}X_{\mu''',\mu''''}^{\mu'',\mu}
$$

$$
\times\langle B_{\mu'''',\mathbf{K}_2}^\dagger B_{\mu',\mathbf{K}_i}^\dagger B_{\mu''',\mathbf{K}_i}\rangle - \frac{1}{\varepsilon V}\sum_{\mu',\mu'',\mu''',i=1,2}\mathbf{G}_{\mu',\mu''}\cdot\mathbf{G}_{\mu''',\mu}\langle B_{\mu''',\mathbf{K}_2}^\dagger B_{\mu',\mathbf{K}_i}^\dagger B_{\mu'',\mathbf{K}_i}\rangle. \tag{3.10}
$$

In addition to the last term that describes excitons scattering off of the grating created via the intraband polarization, there are also a number of PSF terms (terms containing $X_{\mu'',\mu'''}^{\mu',\mu}$). Although most of these PSF terms can be shown to be negligible, the third term may not be. This term is essentially giving the renormalization of the exciton energy due to PSF and may be large at high densities.

## IV. FACTORED DYNAMICAL EQUATIONS

A simplified version of the dynamical equations for DFWM or pump-probe signals arises if one is willing to assume that the triple-operator correlation functions can be factored. This factoring results in a considerable decrease in computational time and also leads to improved physical insight into the dynamical equations.

We factorize $\langle B_{\mu''',\mathbf{K}_n}^\dagger B_{\mu',\mathbf{K}_i}^\dagger B_{\mu'',\mathbf{K}_j}\rangle$ into $\langle B_{\mu',\mathbf{K}_i}^\dagger\rangle$ $\times\langle B_{\mu''',\mathbf{K}_n}^\dagger B_{\mu'',\mathbf{K}_j}\rangle$ or $\langle B_{\mu''',\mathbf{K}_n}^\dagger\rangle\langle B_{\mu',\mathbf{K}_i}^\dagger B_{\mu'',\mathbf{K}_j}\rangle$. The justification for this factorization as opposed to $\langle B_{\mu''',\mathbf{K}_n}^\dagger B_{\mu',\mathbf{K}_i}^\dagger\rangle$ $\times\langle B_{\mu'',\mathbf{K}_j}\rangle$ lies in the physical meaning of $\langle B_{\mu''',\mathbf{K}_n}^\dagger B_{\mu'',\mathbf{K}_j}\rangle$ as an intraband correlation function. This will be nonzero even when only one exciton is present, whereas $\langle B_{\mu''',\mathbf{K}_n}^\dagger B_{\mu',\mathbf{K}_i}^\dagger\rangle$ is associated with biexcitons which are not important in this system.

We consider the equation of motion for $\langle B_{\mu,2\mathbf{K}_2-\mathbf{K}_1}^\dagger\rangle^{(3)}$ which yields the DFWM signal. Using the factorization $\langle B_{\mu''',\mathbf{K}_n}^\dagger B_{\mu',\mathbf{K}_i}^\dagger B_{\mu'',\mathbf{K}_j}\rangle = \langle B_{\mu',\mathbf{K}_i}^\dagger\rangle\langle B_{\mu''',\mathbf{K}_n}^\dagger B_{\mu'',\mathbf{K}_j}\rangle$, the second last term in Eq. (3.9) becomes $E_{\mathbf{K}_1-\mathbf{K}_2}^{\mathrm{intra}(2)}\cdot\Sigma_{\mu'}\mathbf{G}_{\mu',\mu}\langle B_{\mu',\mathbf{K}_2}^\dagger\rangle$, where $E_{\mathbf{K}}^{\mathrm{intra}(2)}\equiv -1/\epsilon\langle P_{\mathbf{K}}^{\mathrm{intra}(2)}\rangle$ is simply the $\mathbf{K}$th Fourier component of the THz field generated by the intraband polarization to second order. As a result of the factoring, we no longer need to compute $\langle B_{\mu,\mathbf{K}_2}^\dagger B_{\mu',\mathbf{K}_2}^\dagger\rangle$ or $\langle B_{\mu,\mathbf{K}_2}^\dagger B_{\mu',\mathbf{K}_2}^\dagger B_{\mu'',\mathbf{K}_1}\rangle$. This results in a huge reduction of computational time, as it is the calculation of $\langle B_{\mu,\mathbf{K}_2}^\dagger B_{\mu',\mathbf{K}_2}^\dagger B_{\mu'',\mathbf{K}_1}\rangle$ that requires the vast majority of the

computational effort in the unfactored equations. Through the factoring procedure, the physics of the source term for the DFWM signal in the $2\mathbf{K}_2-\mathbf{K}_1$ direction becomes clear: the excitons optically created with wave vector $\mathbf{K}_2$ are scattered by the grating created by the intraband cross polarization with wave vector $\mathbf{K}_2-\mathbf{K}_1$ that arises from the excitons created by the two pulses. This term is identical in form to the term that arises from the interaction with the THz field, with the main differences being the order and wave vector of the $\langle B_{\mu',\mathbf{K}}^\dagger\rangle$ factor and the source of the THz field. In the next section, we will show that this factoring procedure can be very accurate.

## V. NUMERICAL RESULTS

The system that we shall model in all of the following is a GaAs/Ga$_{0.7}$Al$_{0.3}$As superlattice with well widths of 67 Å and barrier widths of 17 Å. This is the structure of the superlattice which was studied in many recent DFWM experiments.[35–37] The physical parameters used to model the system (effective masses, band off sets, etc.) are the same as those employed in a number of earlier works.[27,31] The electron miniband width for this system is approximately $\Delta_e = 38$ meV, while the heavy-hole miniband width is $\Delta_h = 3$ meV. The calculations are all done for a dc electric field of $E_{\mathrm{dc}} = 15$ kV/cm and no THz field ($E^{\mathrm{THz}}=0$). This gives a *free-particle* Bloch oscillation period of $\tau_B = 328$ fs, with corresponding WSL level spacing of $\hbar\omega_B = 12.6$ meV.

In general, the quantum number of internal motion $\mu$ labels both the state of motion along the superlattice axis (excitonic WSL index) as well as the in-plane motion. In this work, we consider the response due only to $1s$ heavy-hole excitons. Although the light hole excitons and excitons with higher in-plane energy are included in our formalism, to simplify the calculations we neglect these here; when the excitation is performed with the exciting laser centered below the center of the excitonic WSL ($\omega_c < \omega_0$), it has been shown that the effect of the these other states is small.[31] The basis set used in the calculation of the excitonic states is the so-
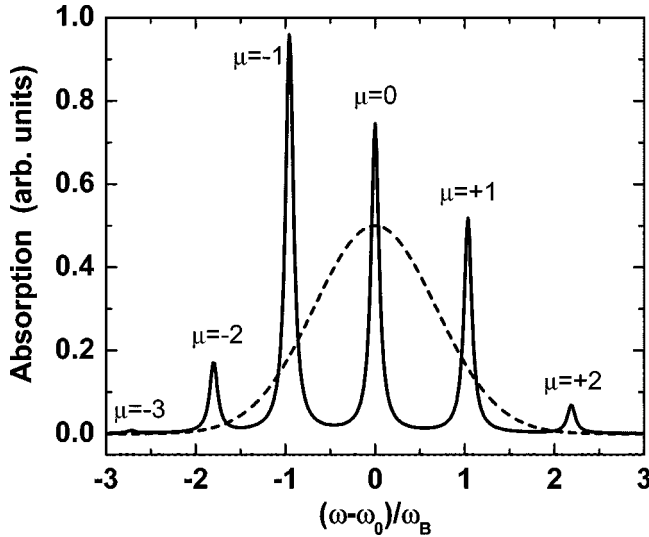
FIG. 1. The calculated absorption spectrum (solid) of the 67/17 superlattice under a bias of 15 kV/cm. Superimposed upon the spectrum (dashed) is the power spectrum of the exciting pulse when its central frequency is at the $\mu=0$ exciton WSL frequency ($\omega_c = \omega_0$). The quantum number $\mu$ of the excitonic WSL state associated with each peak is given above the peak.

called two-well exciton basis that we have employed in a number of earlier works.[14,27,31] This basis set takes account of the exact Coulomb interaction between the electrons and holes and has been shown to produce accurate excitonic energy levels and oscillator strengths.[27] In performing this calculation, we employ a basis set of 11 two-well states ranging in electron-hole separation from $-5d$ to $+5d$. We find that extending the basis set has negligible effect on any of the results presented here.

In Fig. 1 we plot the linear absorption spectrum due to the 1s excitons in this structure under the 15 kV/cm bias. The absorption peaks are labeled by the quantum number $\mu$ of the excitonic WSL state associated with each peak. For such dc field strengths, this quantum number can be thought of as the excitonic analog of the WSL index $n$ for the single-particle WSL; thus the electron-hole separation in the $z$ direction is given approximately by $\mu d$.[27] Also shown on the plot is the power spectrum of one of the exciting pulses when it is centered on the $\mu=0$ WSL state—that is when $\omega_c = \omega_0$.

The experiments being modeled are DFWM experiments, where two pulses are incident on the sample with wave vectors $\mathbf{K}_1$ and $\mathbf{K}_2$, with pulse peaks arriving at times $\tau_1$ and $\tau_2$, respectively, with a temporal separation $\tau_{21} \equiv \tau_2 - \tau_1$. The pulses are Gaussian, with a temporal FWHM of 90 fs (spectral FWHM of 20 meV). The central frequency of the pulses is denoted by $\omega_c$. This takes on different values in the various calculations presented below, but is always chosen so that $\omega_{-2} \leq \omega_c \leq \omega_2$. We set the intensity of the two pulses to be equal and we fix the photoexcited exciton density per superlattice period to be $10^{10}$ cm$^{-2}$ in all instances. This is accomplished by adjusting the optical pulse peak intensity for the pulses.

The phenomenological dephasing times are chosen to

agree with recent experimental results.[45] The interband dephasing time $T_\mu^{(j)} = T_{\text{inter}}$ is set to a value of 1 ps (independent of $\mu$ and $\mathbf{K}$), while the intraband dephasing time $T_{\mu,\mu'}^{(2\bar{1})} = T_{\text{intra}}$ is given a value of 1.5 ps (independent of $\mu, \mu'$, and $\mathbf{K}$). The other dephasing times cannot be so easily gathered from experiment. For the dephasing time $T_{\mu\mu'\mu''}^{(22\bar{1})}$ associated with $\langle B_{\mu,\mathbf{K}_2}^\dagger B_{\mu',\mathbf{K}_2}^\dagger B_{\mu'',\mathbf{K}_1} \rangle$, unless otherwise stated, we use the value that one would obtain in a factored approximation. $T_{\mu\mu'\mu''}^{(22\bar{1})} = T_{\mu\mu'\mu''}^{(22\bar{1})\,\text{fact}}$, where

$$\frac{1}{T_{\mu\mu'\mu''}^{(22\bar{1})\,\text{fact}}} \equiv \frac{1}{T_{\text{inter}}} + \frac{1}{T_{\text{intra}}}. \qquad (5.1)$$

Similarly, we use the result for the factored expression for the dephasing time $T_{\mu,\mu'}^{(22)}$, associated with $\langle B_{\mu,\mathbf{K}_2}^\dagger B_{\mu',\mathbf{K}_2}^\dagger \rangle$: $T_{\mu,\mu'}^{(22)} = T_{\mu,\mu'}^{(22)\,\text{fact}}$, where $T_{\mu,\mu'}^{(22)\,\text{fact}} \equiv \frac{1}{2} T_{\text{inter}}$. Of course, this choice of dephasing times will affect the results and will give the best agreement between the factored and unfactored results. However, as we show shortly, the value of $T_{\mu,\mu'}^{(22)}$ has practically no effect on the results when $\tau_{21} > 0$. Although it is not clear exactly what value should be used for $T_{\mu\mu'\mu''}^{(22\bar{1})}$, we find that essentially the only effect on the time-integrated DFWM signal of changing this time constant is to change the overall intensity of the signal with no significant change in the dependence on $\tau_{21}$. Of course, when the factored equations are used, the only dephasing times that enter the equations are the interband and intraband dephasing times.

In calculating the DFWM intensities, we make the standard approximation and neglect propagation effects. This is valid as long as the number of periods of the superlattice is not too large. In this approximation the DFWM intensity is simply proportional to the absolute value squared of the expectation value of the third-order interband polarization with wave vector $2\mathbf{K}_2 - \mathbf{K}_1$.

In Fig. 2 we plot the time integrated degenerate four-wave mixing (TIFWM) intensity as a function of the time delay $\tau_{21}$ between pulse 2 and pulse 1. This is plotted for six different central laser frequencies. In each plot, we present the results from the unfactored (solid) and factored (dashed) equations. As can be seen, the results from the factored equations are essentially identical to those of the unfactored equations. In most cases, the two lines cannot even be distinguished on this scale.

To make a fair comparison between factored and unfactored results, we must look at the effect of the values used for the time constants $T_{\mu,\mu'}^{(22)}$ and $T_{\mu\mu'\mu''}^{(22\bar{1})}$ on the results. In Fig. 3 we plot the TIFWM signal for the case $\omega_c = \omega_{-2}$ using the factored and unfactored equations. If Fig. 3(a), we examine the effect of $T_{\mu,\mu'}^{(22)}$ on the TIFWM signal. As can be seen, the factored equations yield almost identical results for $\tau_{21} \gtrsim 0$, but the rise time of the signal can differ considerably for $\tau_{21} < 0$ when $T_{\mu,\mu'}^{(22)}$ is far from being equal to $T_{\mu,\mu'}^{(22)\,\text{fact}}$. The measurement of the rise time could thus be used to provide a sensitive measure of the best value for $T_{\mu,\mu'}^{(22)}$. The published experimental TIFWM data for $\tau_{21} < 0$ in BSSL's
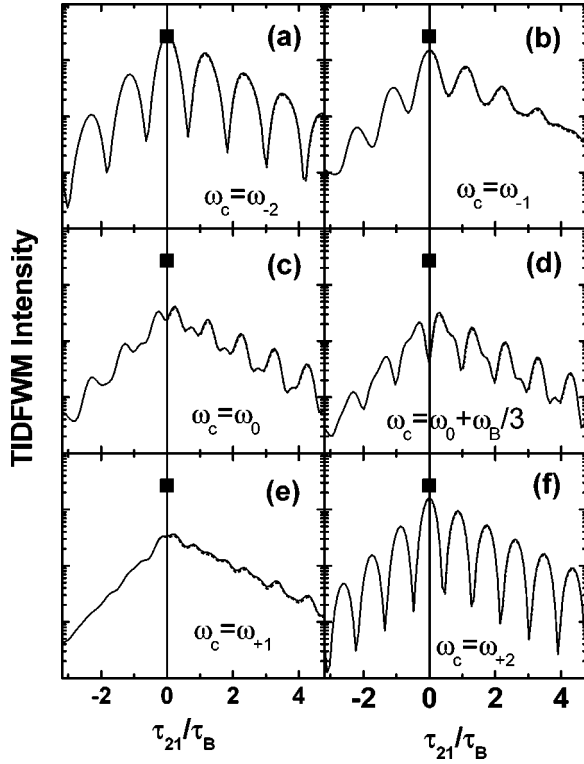
FIG. 2. The calculated TIFWM intensity as a function of the time delay $\tau_{21}$ between pulse 2 and pulse 1 for different central frequencies of the exciting laser. The different plots correspond to central frequencies of (a) $\omega_c = \omega_{-2}$, (b) $\omega_c = \omega_{-1}$, (c) $\omega_c = \omega_0$, (d) $\omega_c = \omega_0 + \omega_B/3$, (e) $\omega_c = \omega_{+1}$, (f) $\omega_c = \omega_{+2}$. In each plot, the solid curve is the result using the full dynamical equations, while the dashed curve is the result using the factored equations. The scale is the same for all plots, and the solid square in each plot marks the maximum intensity found when $\omega_c = \omega_{-2}$.



FIG. 3. The calculated TIFWM intensity as a function of the time delay $\tau_{21}$ between pulse 2 and pulse 1 for $\omega_c = \omega_{-2}$ for different choices of time constants. In (a) we plot curves when $T_{\mu,\mu'}^{(22)}$ takes the values $T_{\mu,\mu'}^{(22)\,\text{fact}}/2$ (dashed), $T_{\mu,\mu'}^{(22)\,\text{fact}}$ (solid), and $2T_{\mu,\mu'}^{(22)\,\text{fact}}$ (dotted), where $T_{\mu\mu'\mu''}^{(22\bar{1})} = T_{\mu\mu'\mu''}^{(22\bar{1})\,\text{fact}}$ in all cases. In (b) we plot curves when $T_{\mu\mu'\mu''}^{(22\bar{1})}$ takes the values $T_{\mu\mu'\mu''}^{(22\bar{1})\,\text{fact}}/2$ (dashed), $T_{\mu\mu'\mu''}^{(22\bar{1})\,\text{fact}}$ (solid), and $2T_{\mu\mu'\mu''}^{(22\bar{1})\,\text{fact}}$ (dotted), where $T_{\mu,\mu'}^{(22)} = T_{\mu,\mu'}^{(22)\,\text{fact}}$ in all cases. To aid in the comparison in (b), we have shifted the curves vertically such that they all coincide at $\tau_{21} = 0$ (see text); the inset shows the curves before shifting.

do not extend far enough in time to obtain a sensitive measure of this rise time.[33] However, it is clear from this data that $T_{\mu,\mu'}^{(22)}$ is not much greater than $T_{\mu,\mu'}^{(22)\,\text{fact}}$, otherwise the signals for $\tau_{21} < 0$ would be much stronger. Also, one would not expect a shorter time than $T_{\mu,\mu'}^{(22)\,\text{fact}}$ as this is a measure of exciton-exciton correlations. Thus, it appears from that available data that $T_{\mu,\mu'}^{(22)} \simeq T_{\mu,\mu'}^{(22)\,\text{fact}}$.

In Fig. 3(b), we examine the effect of $T_{\mu\mu'\mu''}^{(22\bar{1})}$ on the TIFWM signal. In the inset to Fig. 3(b), we have plotted the TIFWM signal for $\omega_c = \omega_{-2}$ for three different values of $T_{\mu\mu'\mu''}^{(22\bar{1})}$. The main effect of changing $T_{\mu\mu'\mu''}^{(22\bar{1})}$ is to change the overall intensity of the signal. Thus, to aid in the comparison, in the main part of Fig. 3(b), we have multiplied curves (a) and (c) by factors of 3 and 1/2.6 so as to make all curves equal at $\tau_{21} = 0$. As can be seen the agreement between the three curves is excellent. Thus, apart from an overall intensity (which is extremely difficult to measure), the factored equations always give excellent results for positive time delays and thus our picture of the intraband polarization driving the TIFWM signal is validated. We have also examined the effect of $T_{\mu\mu'\mu''}^{(22\bar{1})}$ on the time-resolved DFWM signal (not shown). We find that the decay time and overall ampli-
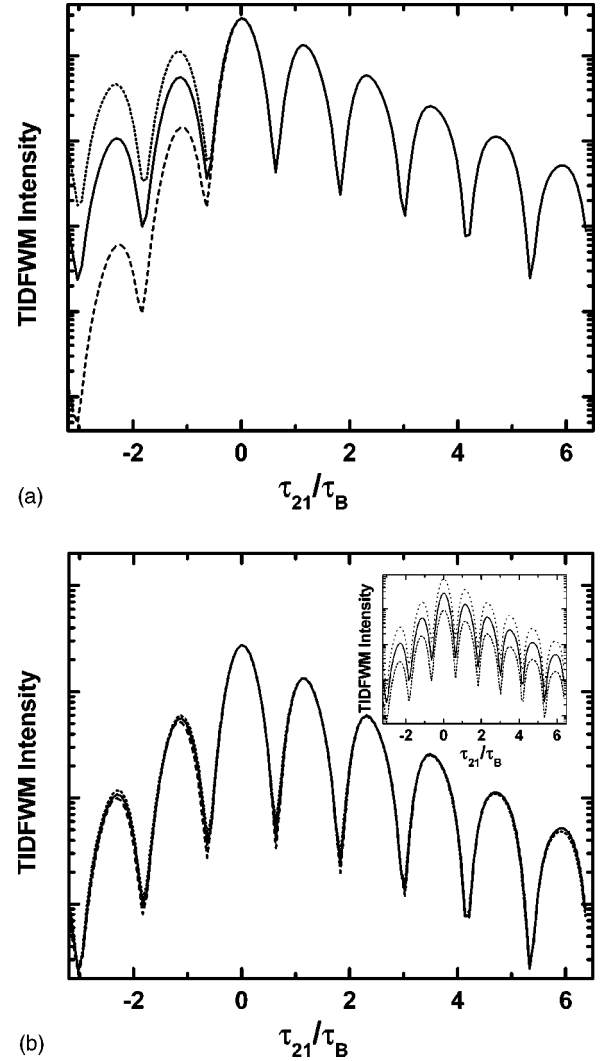
tude are affected by $T_{\mu\mu'\mu''}^{(22\bar{1})}$, but that the general "shape" of the signal is relatively insensitive to this time constant.

Returning to Fig. 2(a), where $\omega_c = \omega_{-2}$ we see the expected oscillations in the intensity that are associated with BO and have been experimentally observed by many authors.[32,33,38,45] As the central laser frequency is increased, the peak intensity of the TIFWM signal decreases [Figs. 2(b), 2(c), and 2(d)]. This decrease arises because the *intraband* polarization with wave vector $\mathbf{K}_2 - \mathbf{K}_1$ is decreasing as the central laser frequency approaches $\omega_0 + \omega_B/3$. As has been discussed both theoretically[31] and experimentally,[35–37] if one ignores the excitonic effects, then when a single laser
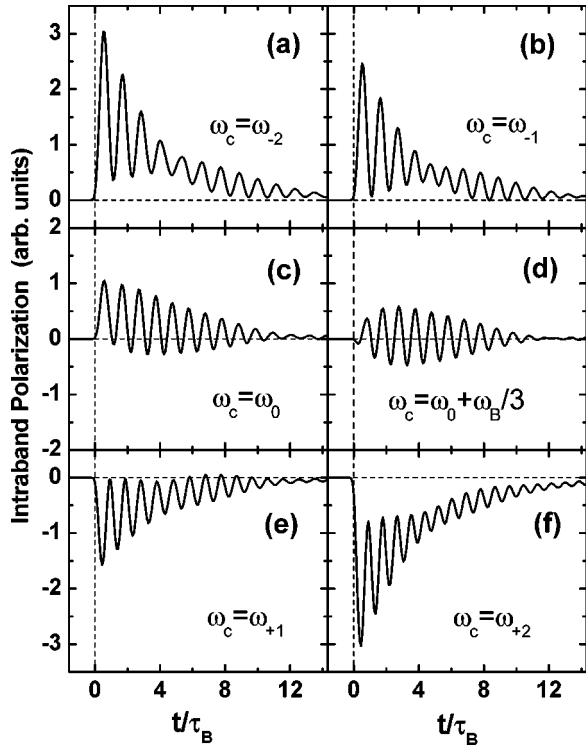
FIG. 4. The calculated intraband polarization with wave vector $\mathbf{K}_2 - \mathbf{K}_1$ as a function of time for zero time delay between the two pulses ($\tau_{21} = 0$). The polarization is plotted at the position $\mathbf{R} = 0$ (see text). The different plots correspond to central frequencies of (a) $\omega_c = \omega_{-2}$, (b) $\omega_c = \omega_{-1}$, (c) $\omega_c = \omega_0$, (d) $\omega_c = \omega_0 + \omega_B/3$, (e) $\omega_c = \omega_{+1}$, (f) $\omega_c = \omega_{+2}$. The scale is the same for all plots, but the origin is shifted.

pulse is applied that is centered at $\omega_c = \omega_0$, the electronic wave packet undergoes an exact breathing mode. When excitonic effects are taken into account,[31] the wave packet no longer undergoes a pure breathing motion, but has some dipolar component. It is found from calculations that the motion is closest to a breathing mode when $\omega_c = \omega_0 + \omega_B/3$.

When the laser is centered away from $\omega_0$ then, even when only say the $\mu$th excitonic WSL state is excited, a dipole is suddenly created by the pulse. This dipole is due to the sudden creation of an electron-hole pair that are separated by approximately $\mu d$. Now, when intraband dephasing is taken into account, this dc dipole will decay. We thus call this the quasi-dc component to the intraband polarization. It will play an important role in the remainder of this section. It is found that the quasi-dc component of the intraband polarization is nearly zero when $\omega_c = \omega_0 + \omega_B/3$–the same laser frequency for which the motion approaches a breathing mode (see Fig. 4).

To demonstrate the dependence of the intraband polarization on $\omega_c$, in Fig. 4 we plot the real part of intraband polarization with wave number $|\mathbf{K}_2 - \mathbf{K}_1|$, denoted by $P_{(2\bar{1})}^{\text{intra}}$, for $\tau_{21} = 0$. We note that there is also a spatially uniform component to the intraband polarization. However, as this does not affect the DFWM signals, we do not consider this here. The intraband polarization is spatially dependent and it is only the $\mathbf{K}_2 - \mathbf{K}_1$ Fourier component that drives the

DFWM signal. Thus, we have to be careful as to what we plot if we are to assess the relative amplitudes of the intraband polarization. Therefore, in Fig. 4 we plot $P_{(2\bar{1})}^{\text{intra}}$ evaluated at the spatial location where the energy density of this polarization is a maximum. When $\tau_{21} = 0$, this simply corresponds to the position $\mathbf{R} = 0$. In general, $P_{(2\bar{1})}^{\text{intra}}$ contains an oscillating portion and a quasi-dc component that initially centers the polarization away from $P_{(2\bar{1})}^{\text{intra}} = 0$. As can be seen in the figure, both the initial oscillation amplitude and the quasi-dc component of $P_{(2\bar{1})}^{\text{intra}}$ is largest for $\omega_c = \omega_{\pm 2}$, and smallest for $\omega_c = \omega_0 + \omega_B/3$. We also see that the quasi-dc component changes sign as expected as one goes from $\omega_c < \omega_0$ to $\omega_c > \omega_0$. Also, from Fig. 4(d) we see that, although the initial polarization amplitude is very small, it grows in time. This is due to the rephasing of the different components that occurs as a result of the different oscillation frequencies arising from differences in the excitonic energy-level spacings.[36]

Note that when $\omega_c = \omega_{-2}$ the BO frequency is considerably higher than when $\omega_c = \omega_{+2}$. This is due to the fact that the excitonic WSL states have a larger energy separation when $\mu > 0$ than when $\mu < 0$, as has been discussed by Lachaine et al.[14] From experimental results,[45] we would expect that this frequency change should also be reflected in the intraband polarization. The THz radiation emitted due to the Bloch-oscillating carriers can be determined by taking the second time derivative of the intraband polarization. Hence, using the results in Figs. 2 and 4, we can compare the oscillation frequencies found in TIFWM calculations with those found in THz emission. It can be seen by inspection of Figs. 1, 2(a), 2(f), 4(a), and 4(f) that when well-defined BO are present the two frequencies are essentially the same and are given by the energy separation of the dominant excitonic peaks for the chosen excitation energy.

Another interesting feature appears when the system is excited near the breathing mode condition. In Figs. 2(c), 2(d), and 2(e), we find that there is a local minimum (dip) at $\tau_{21} = 0$, whereas for the other cases this is a global maximum in the intensity. The appearance of this dip is reminiscent of the dip that was experimentally observed for certain central laser frequencies in the TIFWM signals arising from coherent excitation of light and heavy hole magnetoexcitons in bulk GaAs.[48] The origin for this is again the moving in and out of the breathing-mode condition. In Fig. 5 we plot the intraband polarization $P_{(2\bar{1})}^{\text{intra}}$ when $\omega_c = \omega_0 + \omega_B/3$ for $\tau_{21} = 0$ and $\tau_{21} = \pm \tau_B/2$. As can be seen, both the amplitude and the quasi-dc component of the $P_{(2\bar{1})}^{\text{intra}}$ are much larger when $\tau_{21} = \pm \tau_B/2$ than when $\tau_{21} = 0$. This is because the delay of the second pulse by half a BO period creates a wavepacket with a different phase relationship between the different excitonic states, such that the condition that lead to the breathing motion when $\tau_{21} = 0$ no longer exists and a large-amplitude intraband polarization with large dc component is created. We find that both the ac and quasi-dc components contribute to creating the dip in TRFWM; thus the TIFWM signal is generally large whenever the $P_{(2\bar{1})}^{\text{intra}}$ is large.

As far as we know, the appearance of the dip at $\tau_{21} = 0$ in a BSSL has not been observed experimentally to date. The
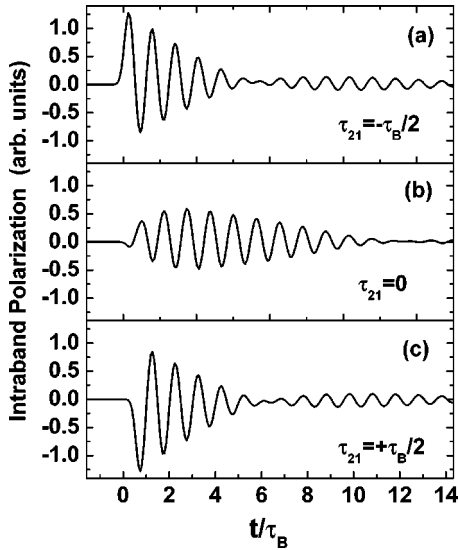
FIG. 5. The calculated intraband polarization with wave vector $\mathbf{K}_2 - \mathbf{K}_1$ as a function of time for a central laser frequency at the near breathing-mode condition $\omega_c = \omega_0 + \omega_B/3$. The polarization is plotted at the position $\mathbf{R}$ for which it is a maximum (see text). The different plots correspond to different time delays between the two pulses (a) $\tau_{21} = -\tau_B/2$, (b) $\tau_{21} = 0$, and (c) $\tau_{21} = +\tau_B/2$. The scale and origin is the same for all plots.
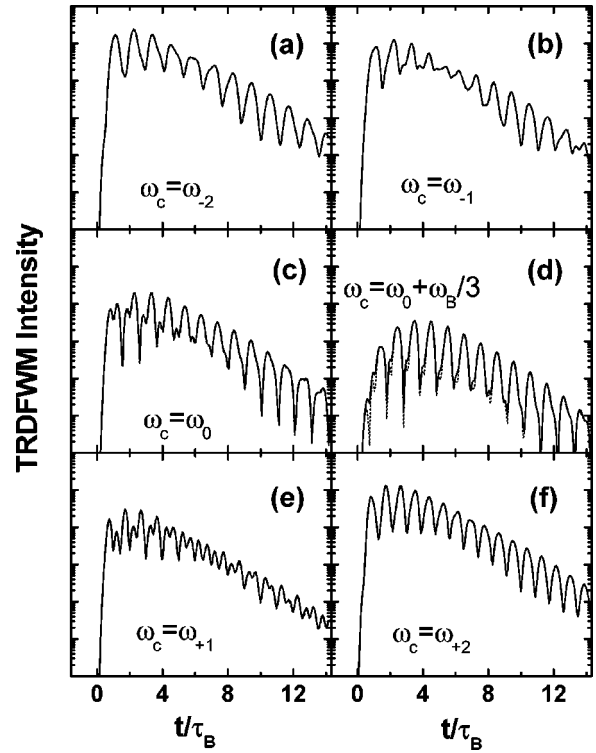


FIG. 6. The calculated time-resolved DFWM intensity as a function of time for zero time delay between the two pulses ($\tau_{21} = 0$). The different plots correspond to central frequencies of (a) $\omega_c = \omega_{-2}$, (b) $\omega_c = \omega_{-1}$, (c) $\omega_c = \omega_0$, (d) $\omega_c = \omega_0 + \omega_B/3$, (e) $\omega_c = \omega_{+1}$, (f) $\omega_c = \omega_{+2}$. The scale is the same for all plots.

reason for this is likely that the effect is masked in experiments by the contributions of the unbound excitonic states that are not included in our calculations. As has been described in previous works,[31] when the laser is centered well below the $\mu = 0$ excitonic state, very few unbound excitonic states are created. However, when $\omega_c \gtrsim \omega_0$ then relatively large numbers of unbound excitons will be created, and the wavepackets formed from these states will not exhibit a breathing mode. To experimentally observe the dip in the TIFWM signal exhibited in our calculations, you would have to remove the portions of the laser spectrum between the 1s excitonic peaks. This is experimentally feasible, but has not been done to date.

We also see that as the condition for a breathing mode is approached, the TIFWM signal exhibits a doubling of the oscillation frequency. Frequency doubling in the TIFWM signal has been observed experimentally[33] at low electric fields, where it is seen to be the result of creating excitonic wavepackets that have strong components from excitonic WSL states that are separated by roughly $2\omega_B$, with a very weak component from the state in between, e.g., the would occur if only the $\mu = -1, +1$ states are part of the wave packet. This effect, however, it has not been observed for the relatively high fields considered here, where the consecutive states are in principle optically created (see Fig. 1). The source of this double-frequency beating is essentially the same as that for the dip: the intraband polarization is sensitive to the time delay $\tau_{21}$. We find in this case that it is largely the quasi-dc component of $P_{(2\bar{1})}^{\text{intra}}$ that generates the frequency doubling. We find (not shown) that when $\tau_{21} = 0$, the quasi-dc component of $P_{(2\bar{1})}^{\text{intra}}$ is small; it is large and positive when $\tau_{21} \simeq \tau_B/2$, small again when $\tau_{21} \simeq \tau_B$, large

and negative when $\tau_{21} \simeq 3\tau_B/2$, and small again when $\tau_{21} \simeq \tau_B$. Thus, the double frequency is associated with the fact that the quasi-dc component of the intraband polarization goes through two minima when $\tau_{21}$ runs over a time $\tau_B$. When we are far from the breathing mode condition [Figs. 2(a), 2(c), 4(a), and 4(c)], the quasi-dc component of the intraband polarization is large enough that it never approaches zero for any $\tau_{21}$. This is why the double frequency is not observed when excitation is far from the breathing-mode condition. As with the dip at $\tau_{21} = 0$, this effect would be masked by the dynamics of the unbound excitons.

To summarize the TIFWM results, we find that when the behavior of the intraband polarization $P_{(2\bar{1})}^{\text{intra}}$ as a function of $\tau_{21}$ is known, one can understand essentially all features of the TIFWM signals. Both the oscillating and quasi-dc parts of $P_{(2\bar{1})}^{\text{intra}}$ play a role in determining the TIFWM peak intensity, oscillation frequency, and signal at $\tau_{21} = 0$. However the quasi-dc portion is of primary importance in determining the appearance of frequency doubling.

In Fig. 6 we present the calculated results for the time-resolved degenerate four wave mixing (TRFWM) intensity for zero time delay ($\tau_{21} = 0$) as a function of time for different central laser frequencies. Again we find only a very small difference between the results from the factored and unfactored equations. The only significant difference is seen for the case that is closest to a breathing mode [Fig. 6(d)], and even in this case the difference only occurs at times when the

DFWM signal intensity is very low. The general effect of the time constants has been discussed earlier.

One interesting feature of the TRFWM results is the dependence of the time required for the signal to reach its global maximum on $\omega_c$. When the intraband polarization is large [Figs. 6(a), 6(b), 6(e), and 6(f)] the maximum is reached in a time of about 0.9 ps, which is approximately $T_{\text{inter}}$. This is in accord with the usual expectations.[49] On the other hand, when we are close to the breathing mode situation, the peak is only reached after about 1.5 ps. This delay in reaching a maximum is due to the delay in the peaking of the intraband polarization, which only peaks after about 1 ps in this case [see Fig. 4(d)].

It is apparent from Fig. 6 that when $\omega_c$ is close to $\omega_0$, both the TIFWM and TRFWM signals exhibits a component at double the BO frequency. The effect here is rather different than that observed in the TIFWM case. It is essentially an *interband* effect and occurs whenever three excitonic states participate in the wave packet with comparable amplitudes. From the factored equation for $\langle B^{\dagger}_{\mu,2\mathbf{K}_2-\mathbf{K}_1}\rangle^{(3)}$, you can see that even if the intraband polarization is essentially dc, you will still get beating at roughly $2\omega_B$ that is comparable to the beating at $\omega_B$ in the TRFWM signal if three consecutive $\langle B^{\dagger}_{\mu',\mathbf{K}_2}\rangle$ are comparable in magnitude. From Fig. 1, you can see that this will only occur if $\omega_c$ is close to $\omega_0$. It will be particularly strong when $\omega_c \simeq \omega_{+1}$ as is observed in the TR-FWM signals. Thus, the fact that this oscillation at double the frequency occurs in the TRFWM signal at nearly the same $\omega_c$ as frequency doubling occurred in the TIFWM signal is essentially a coincidence. It would be possible to choose exciting pulses such that the double frequency would appear for $\omega_c = \omega_{-2}$ without having the double frequency in the TIFWM signal. We thus see that in contrast to the TIFWM signal, the temporal evolution of the TRFWM signal responds largely to interband effects not intraband ones.

## VI. CONCLUSION

In this work we have presented a new formalism for the calculation of DFWM and pump-probe signals in biased asymmetric quantum well systems. The formalism is based on a excitonic approach with interexcitonic interactions treated via the long-wavelength portion of the intraband polarization. The dynamical equations we have developed can be simplified by a factorization scheme that does not lead to the well-known problem of neglecting the important intraexcitonic electron-hole correlations. This factorization is very accurate when $\tau_{21} > 0$, and thus opens the door to the possibility of treating complicated systems to even higher order without running into extreme computational difficulties or computational time limitations. We have applied this formalism to the calculation of the intraband and DFWM signals from a biased semiconductor superlattice, and find in particular that the TIFWM signal is largely determined by the behavior of the intraband polarization.

The numerical results presented here were obtained including only the 1s excitonic states. This is sufficient for many excitation conditions, where it is largely 1s excitons

that are created optically. In future work, however, we plan to extend the basis used in the numerical calculations to include excitons of higher in-plane excitation so as to extend the range of validity of the results. The other main simplification employed in the calculations presented here is the phenomenological treatment of dephasing. Due to the simplification of the basis equations provided by the factoring approximation, it should be possible to incorporate electron-phonon interactions in this calculation without undue computational complexity. We are also currently working towards this result.

## APPENDIX A: EXPRESSION FOR THE INTRA-EXCITONIC COULOMB INTERACTION

In this appendix, we show that in the expression for the Coulomb interaction, we can replace the longitudinal intraband polarization by the full intraband polarization and neglect the contribution of the longitudinal interband polarization. We also show that the long-wavelength portion of the Coulomb interaction does not contribute to the electron-hole interaction energy of a single exciton.

We take the dimensions of the superlattice to be $L_x \times L_y \times L_z$, where $L_z << L_x, L_y$. Let $\mathbf{P}_<(\mathbf{R},t)$ be the form of the long wavelength portion of the polarization within the superlattice. Outside of the superlattice the polarization is taken to be zero. Because the polarization inside the superlattice is generated by the plane-wave optical electric field, we can write it in the form (see Appendix B)

$$\mathbf{P}_<(\mathbf{R},t) = \sum_{\mathbf{K}}^{K<K_M} \mathbf{P}_{\mathbf{K}}(t)e^{i\mathbf{K}\cdot\mathbf{R}}. \tag{A1}$$

Thus, we can express the Fourier transform of the full polarization as

$$\mathcal{P}(\mathbf{k},t) \equiv \frac{1}{(2\pi)^{3/2}} \int d^3\mathbf{R} \, \mathbf{P}_<(\mathbf{R},t)e^{-i\mathbf{k}\cdot\mathbf{R}} \tag{A2}$$

$$= \frac{1}{(2\pi)^{3/2}} \sum_{\mathbf{K}}^{K<K_M} \mathbf{P}_{\mathbf{K}}(t) \sin c[(k_x-K_x)L_x/2]$$

$$\times \sin c[(k_y-K_y)L_y/2]\sin c[(k_z-K_z)L_z/2], \tag{A3}$$

where $\sin c(x) \equiv \sin(x)/x$. From this, we see that $\mathcal{P}(\mathbf{k},t)$ is only appreciable if $|k_i - K_i| < 2\pi/L_i$ for $i=1,2,3$.

The longitudinal portion of the polarization is given by

$$\mathcal{P}_{\parallel}(\mathbf{k},t) = \frac{\mathbf{k}}{k}\left[\frac{\mathbf{k}\cdot\mathcal{P}(\mathbf{k},t)}{k}\right], \tag{A4}$$

where $k=|\mathbf{k}|$. As is shown in Appendix B, the excitonic polarization can be broken into two parts: an intraband por-

tion and an interband portion. We denote these by $\mathbf{P}_{<}^{\text{intra}}(\mathbf{R},t)$ and $\mathbf{P}_{<}^{\text{inter}}(\mathbf{R},t)$, respectively. Let us consider the intraband polarization first. As discussed in Appendix B, due to the symmetry in the $x$-$y$ plane, this only has a $z$ component. Thus, our expression for the longitudinal intraband polarization is simply

$$\mathcal{P}_{\parallel}^{\text{intra}}(\mathbf{k},t) = \frac{\mathbf{k}k_z}{k^2}\mathcal{P}^{\text{intra}}(\mathbf{k},t). \tag{A5}$$

The contribution of this polarization to the Coulomb energy is

$$V_{\text{long}}^{\text{intra}} = \frac{1}{2\varepsilon}\int d^3k\,|\mathcal{P}_{\parallel}^{\text{intra}}(\mathbf{k},t)|^2$$

$$= \frac{1}{(2\pi)^3}\sum_{\mathbf{K},\mathbf{K}'}^{K,K'<K_M}\mathbf{P}_{\mathbf{K}}^{\text{intra}}(t)\cdot\mathbf{P}_{\mathbf{K}'}^{\text{intra}*}(t)\frac{1}{2\varepsilon}$$

$$\times\prod_i\int d^3k\,\frac{k_z^2}{k^2}\sin c[(k_i-K_i)L_i/2]$$

$$\times\sin c[(k_i-K_i')L_i/2]. \tag{A6}$$

In the limit that $L_x,L_y$ become very large we obtain

$$V_{\text{long}}^{\text{intra}} = \frac{1}{4\pi\varepsilon A}\sum_{\mathbf{K},K_z'}^{K,K'<K_M}\mathbf{P}_{\mathbf{K}_{\parallel},K_z}^{\text{intra}}(t)\cdot\mathbf{P}_{\mathbf{K}_{\parallel},K_z'}^{\text{intra}*}(t)$$

$$\times\int dk_z\,\frac{k_z^2}{(K_{\parallel}^2+k_z^2)}\sin c[(k_z-K_z)L_z/2]$$

$$\times\sin c[(k_z-K_z')L_z/2]. \tag{A7}$$

In the actual DFWM experiments of interest, the $\mathbf{K}$ is either zero, or is the difference between two optical photon momenta. Hence in the usual geometry where both beams only make a small angle with the $z$ axis (surface normal) $K_{\parallel}\ll2\pi/\lambda$. Also, if the two optical beams make the same angle with the $z$ axis then $K_z=0$; thus, in general, we have that $K_z\ll2\pi/\lambda$. As an example, consider a superlattice of 30 periods of approximately 7 nm each. Even for this large structure, $L_z\simeq2\times10^{-7}$ m and since $\lambda\simeq800$ nm, $KL_z/2\ll1$. In most AQWS's, such as CDQW's, $L_z$ will not be nearly so large, and so for a general AQWS, we can write

$$\int dk_z\,\frac{k_z^2}{(K_{\parallel}^2+k_z^2)}\sin c[(k_z-K_z)L_z/2]\sin c[(k_z-K_z')L_z/2]$$

$$\simeq\frac{2\pi}{L_z}. \tag{A8}$$

The error in this last expression is easily seen to be less than $\pi K_{\parallel}$. As stated above, this is much less that $2\pi/L_z$ and so is negligible. Thus, we see that we can write

$$V_{\text{long}}^{\text{intra}}\simeq\frac{1}{4\pi\varepsilon A}\sum_{\mathbf{K},K_z'}^{K,K'<K_M}\mathbf{P}_{\mathbf{K}_{\parallel},K_z}^{\text{intra}}(t)\cdot\mathbf{P}_{\mathbf{K}_{\parallel},K_z'}^{\text{intra}*}(t)$$

$$\times\int dk_z\sin c[(k_z-K_z)L_z/2]\sin c[(k_z-K_z')L_z/2]$$

$$= \frac{1}{2\varepsilon}\int d^3\mathbf{R}\,\mathbf{P}_{<}^{\text{intra}}(\mathbf{R},t)\cdot\mathbf{P}_{<}^{\text{intra}}(\mathbf{R},t). \tag{A9}$$

That is, we can replace the longitudinal portion of the intraband polarization by the total polarization. This is the key result of the first part of this appendix.

Next let us consider the interband contribution to $V_{\text{long}}$. As can be seen from Eq. (2.15), the interband polarization is parallel to the bulk interband dipole vector matrix $\mathbf{M}^0$. In GaAs grown in the $\langle100\rangle$ direction, this vector has no $z$-component for heavy-hole excitons. Thus we have for the longitudinal component of the interband polarization

$$\mathcal{P}_{\parallel}^{\text{inter}}(\mathbf{k},t) = \frac{\mathbf{k}k_{\parallel}}{k^2}\mathcal{P}^{\text{inter}}(\mathbf{k},t), \tag{A10}$$

where $k_{\parallel}$ is in the direction of $\mathbf{M}^0$ in the $x$-$y$ plane. In the limit that $L_x,L_y$ become very large, there is only a significant contribution if $k_x\simeq K_x$ and $k_y\simeq K_y$. Hence, similar to what we found above, we see that

$$V_{\text{long}}^{\text{inter}}\simeq\frac{1}{2\pi A}\sum_{\mathbf{K},K_z'}^{K,K'<K_M}\mathbf{P}_{\mathbf{K}_{\parallel},K_z}^{\text{inter}}(t)\cdot\mathbf{P}_{\mathbf{K}_{\parallel},K_z'}^{\text{inter}*}(t)\frac{1}{2\varepsilon}$$

$$\times\int dk_z\,\frac{K_{\parallel}^2}{(K_{\parallel}^2+k_z^2)}\sin c[(k_z-K_z)L_z/2]$$

$$\times\sin c[(k_z-K_z')L_z/2]. \tag{A11}$$

In principle, we could use this expression in our Hamiltonian. However, in the experiments under consideration, the optical beams are nearly parallel to the $z$ axis, and hence they have a very small $K_{\parallel}$. One can show that

$$V_{\text{long}}^{\text{inter}}\leqslant\frac{1}{2\varepsilon V}\sum_{\mathbf{K},K_z'}^{K,K'<K_M}K_{\parallel}L_z\mathbf{P}_{\mathbf{K}_{\parallel},K_z}^{\text{inter}}(t)\cdot\mathbf{P}_{\mathbf{K}_{\parallel},K_z'}^{\text{inter}*}(t).$$

Because $K_{\parallel}L_z\ll1$, we see that $V_{\text{long}}^{\text{inter}}$ is very small. In fact, even without this argument, we know that the interband dipole contributed by an exciton is on the order of $ea$, where $a$ is the lattice constant of GaAs, whereas the intraband contribution of an exciton is on the order of $ed$. Thus the intraband contribution to $V_{\text{long}}$ will generally be much larger than the interband contribution, and in the case of heavy-hole excitons, as we see above it will be negligible. Finally, because the intraband and interband polarizations are orthogonal (for heavy-hole excitons) there are no interband-intraband cross terms in $V_{\text{long}}$. Thus we obtain our final result for the long-wavelength portion of the Coulomb potential

$$V_{\text{long}} = \frac{1}{2\varepsilon}\int d^3\mathbf{R}\,\mathbf{P}_{<}^{\text{intra}}(\mathbf{R},t)\cdot\mathbf{P}_{<}^{\text{intra}}(\mathbf{R},t). \tag{A12}$$

We now consider the issue of whether $V_{\text{long}}$ would contribute to the interaction energy of a single exciton. In our derivation of the Hamiltonian, we replaced $V_{\text{short}}$ by the full $V_{\text{coul}}$ in the single exciton Hamiltonian $H_\gamma^{\text{ex}}$. If this is justified, then we must show that $V_{\text{long}}$ does not contribute to the energy of an individual exciton, as so can be safely added back into to $V_{\text{short}}$ without error. The long-wavelength contribution to Coulomb interaction in the Hamiltonian is given by

$$V_{\text{long}} = \frac{V}{2\varepsilon} \sum_{\mathbf{K}}^{K<K_M} \mathbf{P}_{-\mathbf{K}}^{\text{intra}} \cdot \mathbf{P}_{\mathbf{K}}^{\text{intra}}. \tag{A13}$$

Thus we have

$$V_{\text{long}} = \frac{1}{2\varepsilon V} \sum_{\mathbf{K}',\mathbf{K}''<\mathbf{K}_M} \sum_{\mu,\mu',\mu'',\mu'''} \mathbf{G}_{\mu,\mu'} \cdot \mathbf{G}_{\mu'',\mu'''}$$
$$\times B_{\mu,\mathbf{K}'}^\dagger B_{\mu',\mathbf{K}'-\mathbf{K}} B_{\mu'',\mathbf{K}''}^\dagger B_{\mu''',\mathbf{K}''+\mathbf{K}}. \tag{A14}$$

The state of a single exciton is given simply by

$$|\Psi_{\nu,\mathbf{Q}}\rangle = B_{\nu,\mathbf{Q}}^\dagger |0\rangle. \tag{A15}$$

Thus, if we take the expectation value of $V_{\text{long}}$ for a single exciton, we obtain

$$\langle \Psi_{\nu,\mathbf{Q}} | V_{\text{long}} | \Psi_{\nu,\mathbf{Q}} \rangle = \frac{1}{2\varepsilon V} \mathbf{G}_{\nu,\nu} \cdot \mathbf{G}_{\nu,\nu}. \tag{A16}$$

Now, the $\mathbf{G}_{\nu,\nu}$ are given approximately by

$$\mathbf{G}_{\nu,\nu} \simeq -ed\nu, \tag{A17}$$

where here $\nu d$ gives the average electron-hole separation in the exciton in the $z$ direction. Thus, as long as $\nu$ is finite then in the limit that the volume becomes infinite, the expectation value of $V_{\text{long}}$ will be zero. If $\nu d$ is comparable to the largest dimension of the superlattice, then the expectation value will not go to zero. However, no excitons with such large electron-hole separations will be optically generated, and those that have scattered into such states will no longer contribute to the DFWM signal. The excitons that are generated will have electron-hole separations that are no more than say 400 Å ($3a_0$). The lateral size of the beam is about 50 microns. Thus $(\nu d)^2/A$ will be on the order of $10^{-6}$, and assuming a superlattice that is 50 periods, this gives a value of the expectation value of about $10^{-9}$ eV. Using similar arguments, it is easy to show that there is negligible contribution to the exciton energy at the level of second order perturbation theory as well. Thus, it is justified to include the full $V_{\text{coul}}$ in the single-exciton Hamiltonian in place of $V_{\text{short}}$.

## APPENDIX B: INTRABAND AND INTERBAND POLARIZATION

In this Appendix, we consider the calculation of the polarization. In the dipole approximation the second quantized polarization operator is

$$\mathbf{P}(\mathbf{r}) = -e\psi^\dagger(\mathbf{r})\mathbf{r}\psi(\mathbf{r}), \tag{B1}$$

with

$$\hat{\psi}(\mathbf{r}) = \sum_{b,\mathbf{k}} a_{b,\mathbf{k}} \psi_{b,\mathbf{k}}(\mathbf{r}), \tag{B2}$$

where

$$\psi_{c,\mathbf{k}_e}(\mathbf{r}) = \frac{e^{i\mathbf{k}_{e\|}\cdot\mathbf{r}_\|}}{\sqrt{A}} \phi_{k_{ez}}^c(z) u_c(\mathbf{r}) \tag{B3}$$

and

$$\psi_{v,\mathbf{k}_h}(\mathbf{r}) = \frac{e^{i\mathbf{k}_{h\|}\cdot\mathbf{r}_\|}}{\sqrt{A}} \phi_{k_{hz}}^v(z) u_v(\mathbf{r}) \tag{B4}$$

are the full wave functions for conduction and valence band electrons in the superlattice, respectively, where $u_c(\mathbf{r})$ and $u_v(\mathbf{r})$ are the periodic portion of the bulk wave functions at zone center. The operator $a_{b,\mathbf{k}}$ annihilates an electron in band $b$ with wave vector $\mathbf{k}$, while $\hat{\psi}(\mathbf{r})$ annihilates an electron at $\mathbf{r}$. In the usual way, the polarization operator can be written as

$$\mathbf{P}(\mathbf{r}) = -e \sum_{\mathbf{k},\mathbf{k}'} \alpha_\mathbf{k}^\dagger \alpha_{\mathbf{k}'} \psi_{c,\mathbf{k}}^*(\mathbf{r}) \mathbf{r} \psi_{c,\mathbf{k}'}(\mathbf{r})$$
$$+ e \sum_{\mathbf{k},\mathbf{k}'} \beta_{-\mathbf{k}'}^\dagger \beta_{-\mathbf{k}} \psi_{v,\mathbf{k}}^*(\mathbf{r}) \mathbf{r} \psi_{v,\mathbf{k}'}(\mathbf{r})$$
$$- e \sum_{\mathbf{k},\mathbf{k}'} \alpha_\mathbf{k}^\dagger \beta_{-\mathbf{k}'}^\dagger \psi_{c,\mathbf{k}}^*(\mathbf{r}) \mathbf{r} \psi_{v,\mathbf{k}'}(\mathbf{r})$$
$$- e \sum_{\mathbf{k},\mathbf{k}'} \beta_{-\mathbf{k}} \alpha_{\mathbf{k}'} \psi_{v,\mathbf{k}}^*(\mathbf{r}) \mathbf{r} \psi_{c,\mathbf{k}'}(\mathbf{r})$$
$$- e \sum_{\mathbf{k}} \psi_{v,\mathbf{k}}^*(\mathbf{r}) \mathbf{r} \psi_{v,\mathbf{k}}(\mathbf{r}), \tag{B5}$$

where $\alpha_\mathbf{k}^\dagger = a_c^\dagger,\mathbf{k}$, creates an electron in the CB and $\beta_{-\mathbf{k}}^\dagger \equiv a_{v,\mathbf{k}}$ creates a hole in the VB. The the last term of Eq. (B5) is an arbitrary constant which will be omitted from here on, as it does not affect the dynamics.

The transformations between the electron and hole operators and the electron-hole operators $B_{\mathbf{k}_e,\mathbf{k}_h}^\dagger$ are given by Hawton and Nelson:[23]

$$B_{\mathbf{k}_e,\mathbf{k}_h}^\dagger = \alpha_{\mathbf{k}_e}^\dagger \beta_{\mathbf{k}_h}^\dagger, \tag{B6}$$

$$\alpha_\mathbf{k}^\dagger \alpha_{\mathbf{k}'} = \sum_{\mathbf{k}_h} B_{\mathbf{k},\mathbf{k}_h}^\dagger B_{\mathbf{k}',\mathbf{k}_h}, \tag{B7}$$

and

$$\beta_\mathbf{k}^\dagger \beta_{\mathbf{k}'} = \sum_{\mathbf{k}_e} B_{\mathbf{k}_e,\mathbf{k}}^\dagger B_{\mathbf{k}_e,\mathbf{k}'}, \tag{B8}$$

where $B_{\mathbf{k}_e,\mathbf{k}_h}^\dagger$ creates an electron-hole pair where the electron (hole) has wave vector $\mathbf{k}_e$ ($\mathbf{k}_h$). Thus, in terms of these pair operators the polarization becomes

$$\mathbf{P}(\mathbf{r}) = -e \sum_{\mathbf{k}_e, \mathbf{k}_h} B^{\dagger}_{\mathbf{k}_e, \mathbf{k}_h} \psi^*_{c, \mathbf{k}_e}(\mathbf{r}) \mathbf{r} \psi_{v, -\mathbf{k}_h}(\mathbf{r})$$

$$- e \sum_{\mathbf{k}_e, \mathbf{k}_h} B_{\mathbf{k}_e, \mathbf{k}_h} \psi^*_{v, -\mathbf{k}_h}(\mathbf{r}) \mathbf{r} \psi_{c, \mathbf{k}_e}(\mathbf{r})$$

$$- e \sum_{\mathbf{k}_e, \mathbf{k}_h, \mathbf{k}'_e} B^{\dagger}_{\mathbf{k}_e, \mathbf{k}_h} B_{\mathbf{k}'_e, \mathbf{k}_h} \psi^*_{c, \mathbf{k}_e}(\mathbf{r}) \mathbf{r} \psi_{c, \mathbf{k}'_e}(\mathbf{r})$$

$$+ e \sum_{\mathbf{k}_e, \mathbf{k}_h, \mathbf{k}'_h} B^{\dagger}_{\mathbf{k}_e, \mathbf{k}_h} B_{\mathbf{k}_e, \mathbf{k}'_h} \psi^*_{v, -\mathbf{k}'_h}(\mathbf{r}) \mathbf{r} \psi_{v, -\mathbf{k}_h}(\mathbf{r}). \tag{B9}$$

Finally, we move to the true exciton operators $B^{\dagger}_{\mu, \mathbf{K}}$ through the relations

$$B^{\dagger}_{\mu, \mathbf{K}} = \sum_{\mathbf{k}} \psi^{\mu, \mathbf{K}}_{\mathbf{k}} B^{\dagger}_{\mathbf{k}, \mathbf{K}} \tag{B10}$$

and the inverse transformation

$$B^{\dagger}_{\mathbf{k}, \mathbf{K}} = \sum_{\mu} (\psi^{\mu, \mathbf{K}}_{\mathbf{k}})^* B^{\dagger}_{\mu, \mathbf{K}}, \tag{B11}$$

where $B^{\dagger}_{\mu, \mathbf{K}}$ creates an exciton with envelope function

$$\tilde{\Psi}_{\mu', \mathbf{K}}(\mathbf{r}; \mathbf{R}) = \Psi_{\mu, \mathbf{K}}(\mathbf{r}_e; \mathbf{r}_h)$$

$$\equiv \sum_{\mathbf{k}} \psi^{\mu, \mathbf{K}}_{\mathbf{k}} \frac{e^{i\mathbf{k}_{e\parallel} \cdot \mathbf{r}_e}}{\sqrt{A}} \phi^c_{k_{ez}}(z_e) \frac{e^{i\mathbf{k}_{h\parallel} \cdot \mathbf{r}_h}}{\sqrt{A}} \phi^{v*}_{-k_{hz}}(z_h), \tag{B12}$$

where $\psi^{\mu, \mathbf{K}}_{\mathbf{k}}$ are the expansion coefficients, $\phi^c_{k_{ez}}(z_e)$ $[\phi^v_{k_{hz}}(z_h)]$ is the conduction-band (valence-band) electron envelope function for the superlattice in the $z$ direction, $\mathbf{K} = \mathbf{k}_e + \mathbf{k}_h$ is the center-of-mass wave vector of the exciton and $\mathbf{k} = (m_h \mathbf{k}_e - m_e \mathbf{k}_h)/M$ is the relative electron-hole wave vector, where $M = m_e + m_h$. We can also define the electron hole separation coordinate $\mathbf{r} = \mathbf{r}_e - \mathbf{r}_h$ and center-of-mass coordinates $\mathbf{R} = (m_e \mathbf{r}_e + m_h \mathbf{r}_h)/M$. Using this transformation, we obtain the following expression for the polarization operator

$$\mathbf{P}(\mathbf{r}) = -e \sum_{\mu} \sum_{\mathbf{k}, \mathbf{K}'} \psi^{\mu, \mathbf{K}'*}_{\mathbf{k}} B^{\dagger}_{\mu, \mathbf{K}'} \psi^*_{c, \gamma_e \mathbf{K}' + \mathbf{k}}(\mathbf{r})$$

$$\times \mathbf{r} \psi_{v, -\gamma_h \mathbf{K}' + \mathbf{k}}(\mathbf{r})$$

$$- e \sum_{\mu} \sum_{\mathbf{k}, \mathbf{K}'} \psi^{\mu, \mathbf{K}'}_{\mathbf{k}} B_{\mu, \mathbf{K}'} \psi^*_{v, -\gamma_h \mathbf{K}' + \mathbf{k}}(\mathbf{r})$$

$$\times \mathbf{r} \psi_{c, \gamma_e \mathbf{K}' + \mathbf{k}}(\mathbf{r})$$

$$- e \sum_{\mu, \mu'} \sum_{\mathbf{k}_e, \mathbf{k}_h, \mathbf{k}'_e} \psi^{\mu, \mathbf{k}_e + \mathbf{k}_h*}_{\gamma_h \mathbf{k}_e - \gamma_e \mathbf{k}_h} \psi^{\mu', \mathbf{k}'_e + \mathbf{k}_h}_{\gamma_h \mathbf{k}'_e - \gamma_e \mathbf{k}_h} B^{\dagger}_{\mu, \mathbf{k}_e + \mathbf{k}_h}$$

$$\times B_{\mu', \mathbf{k}'_e + \mathbf{k}_h} \psi^*_{c, \mathbf{k}_e}(\mathbf{r}) \mathbf{r} \psi_{c, \mathbf{k}'_e}(\mathbf{r})$$

$$+ e \sum_{\mu, \mu'} \sum_{\mathbf{k}_e, \mathbf{k}_h, \mathbf{k}'_h} \psi^{\mu, \mathbf{k}_e + \mathbf{k}_h*}_{\gamma_h \mathbf{k}_e - \gamma_e \mathbf{k}_h} \psi^{\mu', \mathbf{k}_e + \mathbf{k}'_h}_{\gamma_h \mathbf{k}_e - \gamma_e \mathbf{k}'_h} B^{\dagger}_{\mu, \mathbf{k}_e + \mathbf{k}_h}$$

$$\times B_{\mu', \mathbf{k}_e + \mathbf{k}'_h} \psi^*_{v, -\mathbf{k}'_h}(\mathbf{r}) \mathbf{r} \psi_{v, -\mathbf{k}_h}(\mathbf{r}). \tag{B13}$$

The $\mathbf{K}$th Fourier component of the polarization operator is thus defined as

$$\mathbf{P}_{\mathbf{K}} = \frac{1}{V} \int d^3\mathbf{r} \, \mathbf{P}(\mathbf{r}) e^{-i\mathbf{K} \cdot \mathbf{r}}. \tag{B14}$$

Thus the polarization in the long-wavelength limit is given simply by

$$\mathbf{P}_<(\mathbf{R}) = \sum_{\mathbf{K}}^{K < K_M} \mathbf{P}_{\mathbf{K}} e^{i\mathbf{K} \cdot \mathbf{R}}, \tag{B15}$$

where the sum is restricted to include only $\mathbf{K}$ that correspond to long wavelengths ($|\mathbf{K}| < |\mathbf{K}_M|$). The Fourier components of the polarization can be written as the sum of the interband and intraband polarizations

$$\mathbf{P}_{\mathbf{K}} = \mathbf{P}^{\text{inter}}_{\mathbf{K}} + \mathbf{P}^{\text{intra}}_{\mathbf{K}}, \tag{B16}$$

where

$$\mathbf{P}^{\text{inter}}_{\mathbf{K}} = -\frac{e}{V} \sum_{\mu} \sum_{\mathbf{k}, \mathbf{K}'} \psi^{\mu, \mathbf{K}'*}_{\mathbf{k}} B^{\dagger}_{\mu, \mathbf{K}'}$$

$$\times \int d^3\mathbf{r} \psi^*_{c, \gamma_e \mathbf{K}' + \mathbf{k}}(\mathbf{r}) \mathbf{r} \psi_{v, -\gamma_h \mathbf{K}' + \mathbf{k}}(\mathbf{r}) e^{-i\mathbf{K} \cdot \mathbf{r}}$$

$$- \frac{e}{V} \sum_{\mu} \sum_{\mathbf{k}, \mathbf{K}'} \psi^{\mu, \mathbf{K}'}_{\mathbf{k}} B_{\mu, \mathbf{K}'}$$

$$\times \int d^3\mathbf{r} \psi^*_{v, -\gamma_h \mathbf{K}' + \mathbf{k}}(\mathbf{r}) \mathbf{r} \psi_{c, \gamma_e \mathbf{K}' + \mathbf{k}}(\mathbf{r}) e^{-i\mathbf{K} \cdot \mathbf{r}} \tag{B17}$$

is the interband portion of the polarization and

$$\mathbf{P}^{\text{intra}}_{\mathbf{K}} = -\frac{e}{V} \sum_{\mu, \mu'} \sum_{\mathbf{k}_e, \mathbf{k}_h, \mathbf{k}'_e} \psi^{\mu, \mathbf{k}_e + \mathbf{k}_h*}_{\gamma_h \mathbf{k}_e - \gamma_e \mathbf{k}_h} \psi^{\mu', \mathbf{k}'_e + \mathbf{k}_h}_{\gamma_h \mathbf{k}'_e - \gamma_e \mathbf{k}_h} B^{\dagger}_{\mu, \mathbf{k}_e + \mathbf{k}_h}$$

$$\times B_{\mu', \mathbf{k}'_e + \mathbf{k}_h} \int d^3\mathbf{r}_e \psi^*_{c, \mathbf{k}_e}(\mathbf{r}_e) \mathbf{r}_e \psi_{c, \mathbf{k}'_e}(\mathbf{r}_e) e^{-i\mathbf{K} \cdot \mathbf{r}_e}$$

$$+ \frac{e}{V} \sum_{\mu, \mu'} \sum_{\mathbf{k}_e, \mathbf{k}_h, \mathbf{k}'_h} \psi^{\mu, \mathbf{k}_e + \mathbf{k}_h*}_{\gamma_h \mathbf{k}_e - \gamma_e \mathbf{k}_h} \psi^{\mu', \mathbf{k}_e + \mathbf{k}'_h}_{\gamma_h \mathbf{k}_e - \gamma_e \mathbf{k}'_h} B^{\dagger}_{\mu, \mathbf{k}_e + \mathbf{k}_h}$$

$$\times B_{\mu', \mathbf{k}_e + \mathbf{k}'_h}$$

$$\times \int d^3\mathbf{r}_h \psi^*_{v, -\mathbf{k}'_h}(\mathbf{r}_h) \mathbf{r}_h \psi_{v, -\mathbf{k}_h}(\mathbf{r}_h) e^{-i\mathbf{K} \cdot \mathbf{r}_h} \tag{B18}$$

is the intraband portion.

The Fourier components of the interband polarization may be written in the form

$$\mathbf{P}_{\mathbf{K}}^{\text{inter}} = \frac{1}{V} \sum_{\mu, \mathbf{K}'} \mathbf{M}_{\mu, \mathbf{K}'}^{\mathbf{K}} B_{\mu, \mathbf{K}'}^{\dagger} + \frac{1}{V} \sum_{\mu, \mathbf{K}'} \mathbf{M}_{\mu, \mathbf{K}'}^{-\mathbf{K}*} B_{\mu, \mathbf{K}'},$$

(B19)

where the interband dipole matrix element is given by

$$\mathbf{M}_{\mu, \mathbf{K}'}^{\mathbf{K}} \equiv -e \sum_{\mathbf{k}} \psi_{\mathbf{k}}^{\mu, \mathbf{K}'*}$$

$$\times \int d^3 \mathbf{r} \psi_{c, \gamma_e \mathbf{K}' + \mathbf{k}}^*(\mathbf{r}) \mathbf{r} \psi_{v, \gamma_h \mathbf{K}' - \mathbf{k}}(\mathbf{r}) e^{-i\mathbf{K} \cdot \mathbf{r}}.$$

(B20)

Using standard methods of envelope function theory, is it straight forward to show that this can be written as

$$\mathbf{M}_{\mu, \mathbf{K}'}^{\mathbf{K}} = \delta_{-\mathbf{K}, \mathbf{K}'} \mathbf{M}_{\mu}^{\mathbf{K}},$$

(B21)

where

$$\mathbf{M}_{\mu}^{\mathbf{K}} \equiv \mathbf{M}_0 A \int dz \Psi_{\mu, \mathbf{K}}^*(0, 0, z; 0, 0, z)$$

(B22)

and $\mathbf{M}_0$ is the bulk dipole interband matrix element, defined by

$$\mathbf{M}_0 \equiv e \frac{i\hbar \mathbf{p}_{cv}}{E_{\text{gap}} m_0},$$

(B23)

where

$$\mathbf{p}_{vc} \equiv \frac{1}{V} \int d^3 \mathbf{r} u_c^*(\mathbf{r}_h) \mathbf{p} u_v(\mathbf{r}).$$

(B24)

Now, the excitonic envelop function can be written as

$$\Psi_{\mu, \mathbf{K}}(\mathbf{r}_e; \mathbf{r}_h) = \frac{e^{i\mathbf{K}_{\parallel} \cdot \mathbf{R}_{\parallel}}}{\sqrt{A}} \chi_{\mu, K_z}(\mathbf{r}_{\parallel}; Z, z).$$

(B25)

Using this we can write the exciton dipole matrix element as

$$\mathbf{M}_{\mu}^{\mathbf{K}} = \mathbf{M}_0 \sqrt{A} \int dZ \chi_{\mu, K_z}^*(\mathbf{r}_{\parallel} = 0; Z, z = 0).$$

(B26)

We note that in practice, the dependence of $\mathbf{M}_{\mu}^{\mathbf{K}}$ on $\mathbf{K}$ is very weak and in fact, in the bulk case it is independent of $\mathbf{K}$. We therefore neglect this dependence in actual calculations. Thus, the interband polarization is finally given by

$$\mathbf{P}_{\mathbf{K}}^{\text{inter}} = \sum_{\mu} [\mathbf{M}_{\mu} B_{\mu, -\mathbf{K}}^{\dagger} + \mathbf{M}_{\mu}^* B_{\mu, \mathbf{K}}].$$

(B27)

Now, we turn our attention to the intraband portion of the polarization. Using the relation

$$\delta_{\mathbf{k}, \mathbf{k}'} = \int d^3 \mathbf{r} \psi_{b, \mathbf{k}'}^*(\mathbf{r}) \psi_{b, \mathbf{k}}(\mathbf{r})$$

(B28)

for $b = v$ or $b = c$, this becomes

$$\mathbf{P}_{\mathbf{K}}^{\text{intra}} = -\frac{e}{V} \sum_{\mu, \mu'} \sum_{\mathbf{K}', \mathbf{K}''} B_{\mu, \mathbf{K}'}^{\dagger} B_{\mu', \mathbf{K}''}$$

$$\times \int d^3 \mathbf{r}_e d^3 \mathbf{r}_h \Psi_{\mu, \mathbf{K}'}^*(\mathbf{r}_e; \mathbf{r}_h) |u_c(\mathbf{r}_e)|^2 |u_v(\mathbf{r}_h)|^2$$

$$\times [\mathbf{r}_e e^{-i\mathbf{K} \cdot \mathbf{r}_e} - \mathbf{r}_h e^{-i\mathbf{K} \cdot \mathbf{r}_h}] \Psi_{\mu', \mathbf{K}''}(\mathbf{r}_e; \mathbf{r}_h).$$

(B29)

Using standard methods, we can rewrite this as

$$\mathbf{P}_{\mathbf{K}}^{\text{intra}} = -\frac{e}{V} \sum_{\mu, \mu'} \sum_{\mathbf{K}', \mathbf{K}''} B_{\mu, \mathbf{K}'}^{\dagger} B_{\mu', \mathbf{K}''}$$

$$\times \int d^3 \mathbf{r}_h d^3 \mathbf{r}_h e^{-i\mathbf{K} \cdot \mathbf{R}} \Psi_{\mu, \mathbf{K}'}^*(\mathbf{r}_e; \mathbf{r}_h)$$

$$\times [(\gamma_h \mathbf{r} + \mathbf{R}) e^{-i\mathbf{K} \cdot \gamma_h \mathbf{r}} - (-\gamma_e \mathbf{r} + \mathbf{R}) e^{+i\mathbf{K} \cdot \gamma_e \mathbf{r}}]$$

$$\times \Psi_{\mu', \mathbf{K}''}(\mathbf{r}_e; \mathbf{r}_h).$$

(B30)

This is a general result. However, if we are only considering bound excitons, then the integrand in the above expression will be negligible unless $|\mathbf{r}| \lesssim a_0$, where $a_0$ is the exciton Bohr radius. For higher bound states the exciton may extend over many Bohr radii, but regardless, they will generally satisfy the inequality $\mathbf{K} \cdot \mathbf{r} \ll 1$ for the long-wavelength wave vectors that we are considering. Thus, for bound excitons, we obtain

$$\mathbf{P}_{\mathbf{K}}^{\text{intra}} \simeq -\frac{e}{V} \sum_{\mu, \mu'} \sum_{\mathbf{K}', \mathbf{K}''} B_{\mu, \mathbf{K}'}^{\dagger} B_{\mu', \mathbf{K}''}$$

$$\times \int d^3 \mathbf{r}_h d^3 \mathbf{r}_h e^{-i\mathbf{K} \cdot \mathbf{R}} \Psi_{\mu, \mathbf{K}'}^*(\mathbf{r}_e; \mathbf{r}_h) \mathbf{r} \Psi_{\mu', \mathbf{K}''}(\mathbf{r}_e; \mathbf{r}_h).$$

(B31)

Using Eq. (B25) for the exciton envelope function, we finally obtain

$$\mathbf{P}_{\mathbf{K}}^{\text{intra}} = \frac{1}{V} \sum_{\mu, \mu'} \mathbf{G}_{\mu, \mu'} \sum_{\mathbf{K}'} B_{\mu, \mathbf{K}'}^{\dagger} B_{\mu', \mathbf{K} + \mathbf{K}'},$$

(B32)

where

$$\mathbf{G}_{\mu, \mu'} \equiv -e \int d^3 \mathbf{r} dZ \chi_{\mu, 0}^*(\mathbf{r}_{\parallel}; Z, z) \mathbf{r} \chi_{\mu', 0}(\mathbf{r}_{\parallel}; Z, z)$$

(B33)

and the $K_z$ dependence in the $\chi_{\mu, K_z}(\mathbf{r}_{\parallel}; Z, z)$ have been neglected in the same way that one neglects the wave vector dependence in the $u_{\mathbf{k}}^c(\mathbf{r})$ in standard envelope function theory. This result can also be extended to unbound excitons. In this case, it is easily seen that then we obtain the same expression for $\mathbf{P}_{\mathbf{K}}^{\text{intra}}$ except that the intraband matrix element is dependent on $\mathbf{K}$ and has a more complicated form than given by Eq. (B33). Thus the general form for the intraband polarization for both bound and unbound excitons is

$$\mathbf{P}_{\mathbf{K}}^{\text{intra}} = \frac{1}{V} \sum_{\mu, \mu'} \mathbf{G}_{\mu, \mu'}^{\mathbf{K}} \sum_{\mathbf{K}'} B_{\mu, \mathbf{K}'}^{\dagger} B_{\mu', \mathbf{K} + \mathbf{K}'}.$$

(B34)

We finally note that if we are only considering optically ex-

cited bound excitonic states, then all of the states being considered will have $s$ symmetry in the transverse direction. Thus, for such states, only the $z$ component of $\mathbf{G}_{\mu,\mu'}$ (which we denote by $G_{\mu,\mu'}$ for simplicity) can be nonzero, and this will only be nonzero if there is an applied electric field to break the symmetry in the $z$ direction. If we are considering states with other symmetries, however, then in general all components of $\mathbf{G}_{\mu,\mu'}$ may be nonzero.

---

*Electronic address: dignam@physics.queensu.ca

†Electronic address: margaret.hawton@lakeheadu.ca

[1] S. Schmitt-Rink and D.S. Chemla, Phys. Rev. Lett. **57**, 2752 (1986).

[2] S. Schmitt-Rink, D.S. Chemla, and H. Haug, Phys. Rev. B **37**, 941 (1988).

[3] M. Lindberg and S.W. Koch, Phys. Rev. B **38**, 3342 (1988).

[4] M. Lindberg, R. Binder, and S.W. Koch, Phys. Rev. A **45**, 1865 (1992).

[5] V.M. Axt and A. Stahl, Z. Phys. B: Condens. Matter **93**, 195 (1994); K. Victor, V.M. Axt, and A. Stahl, Phys. Rev. B **51**, 14 164 (1995).

[6] V.M. Axt, G. Bartels, and A. Stahl, Phys. Rev. Lett. **76**, 2543 (1996).

[7] Th. Östreich, K. Schönhammer, and L.J. Sham, Phys. Rev. B **58**, 12 920 (1998).

[8] Th. Östreich, N. Donlagic, C. Wohler, and K. Schönhammer, Phys. Status Solidi B **206**, 205 (1998).

[9] R. Binder, S.W. Koch, M. Lindberg, W. Schäfer, and F. Jahnke, Phys. Rev. B **43**, 6520 (1991).

[10] G. Bartels, G.C. Cho, T. Dekorsy, H. Kurz, A. Stahl, and K. Köhler, Phys. Rev. B **55**, 16 404 (1997).

[11] C. Sieh, T. Meier, F. Jahnke, A. Knorr, S.W. Koch, P. Brick, M. Hübner, C. Ell, J. Prineas, G. Khitrova, and H.M. Gibbs, Phys. Rev. Lett. **82**, 3112 (1999); C. Sieh, T. Meier, A. Knorr, F. Jahnke, P. Thomas, and S.W. Koch, Eur. Phys. J. B **11**, 407 (1999).

[12] T. Meier, S.W. Koch, P. Brick, C. Ell, G. Khitrova, and H.M. Gibbs, Phys. Rev. B **62**, 4218 (2000).

[13] Thomas Östreich, Phys. Rev. B **64**, 245203 (2001).

[14] J.M. Lachaine, Margaret Hawton, J.E. Sipe, and M.M. Dignam, Phys. Rev. B **62**, R4829 (2000).

[15] W. Schäfer, D.S. Kim, J. Shah, T.C. Damen, J.E. Cunningham, K.W. Goossen, L.N. Pfeiffer, and K. Köhler, Phys. Rev. B **53**, 16 429 (1998).

[16] S.W. Koch, T. Meier, F. Jahnke, and P. Thomas, Appl. Phys. A: Mater. Sci. Process. **71**, 511 (2000).

[17] V.M. Axt, K. Victor, and T. Kuhn, Phys. Status Solidi B **206**, 189 (1998).

[18] Wei Min Zhang, Torsten Meier, Vladimir Chernyak, and Shaul Mukamel, Phys. Rev. B **60**, 2599 (1999).

[19] D. Brinkmann, K. Bott, S.W. Koch, and P. Thomas, Phys. Status Solidi B **206**, 493 (1998).

[20] B. Haase, U. Neukirch, J. Gutowski, G. Bartels, A. Stahl, V.M. Axt, J. Nürnberger, and W. Faschinger, Phys. Rev. B **59**, R7805 (1999).

[21] S. Yokojima, T. Meier, V. Chernyak, and S. Mukamel, Phys. Rev. B **59**, 12 584 (1999).

[22] V.M. Axt and S. Mukamel, Rev. Mod. Phys. **70**, 145 (1998).

[23] Margaret Hawton and Delene Nelson, Phys. Rev. B **57**, 4000 (1998).

[24] T.V. Shahbazyan, N. Primozich, and I.E. Perakis, Phys. Rev. B **62**, 15 925 (2000).

[25] Paula Feuer, Phys. Rev. **88**, 92 (1952).

[26] E.E. Mendez, F. Agulló-Rueda, and J.M. Hong, Phys. Rev. Lett. **60**, 2426 (1988).

[27] M.M. Dignam and J.E. Sipe, Phys. Rev. Lett. **64**, 1797 (1991); M.M. Dignam and J.E. Sipe, Phys. Rev. B **43**, 4097 (1991).

[28] D.M. Whittaker, Phys. Rev. B **41**, 3238 (1990); D.M. Whittaker, Europhys. Lett. **31**, 55 (1995).

[29] N. Linder, Phys. Rev. B **55**, 13 664 (1997).

[30] S. Glutsch, P. Lefebvre, and D.S. Chemla, Phys. Rev. B **55**, 15 786 (1997).

[31] M. Dignam, J.E. Sipe, and J. Shah, Phys. Rev. B **49**, 10 502 (1994).

[32] J. Feldmann, K. Leo, J. Shah, D.A.B. Miller, J.E. Cunningham, T. Meier, G. von Plessen, A. Schulze, P. Thomas, and S. Schmitt-Rink, Phys. Rev. B **46**, 7252 (1992).

[33] P. Leisching, P. Haring Bolivar, W. Beck, Y. Dhaibi, F. Brüggemann, R. Schwedler, H. Kurz, K. Leo, and K. Köhler, Phys. Rev. B **50**, 14 389 (1994).

[34] C. Waschke, H.G. Roskos, R. Schwedler, K. Leo, H. Kurz, and K. Köhler, Phys. Rev. Lett. **70**, 3319 (1993).

[35] V.G. Lyssenko, G. Valušis, F. Löser, T. Hasche, K. Leo, M.M. Dignam, and K. Köhler, Phys. Rev. Lett. **79**, 301 (1997).

[36] M. Sudzius, V.G. Lyssenko, F. Löser, K. Leo, M.M. Dignam, and K. Köhler, Phys. Rev. B **57**, R12 693 (1998).

[37] F. Löser, M.M. Dignam, Yu.A. Kosevich, K. Köhler, and K. Leo, Phys. Rev. Lett. **85**, 4763 (2000).

[38] H.J. Bakker, T. Dekorsy, G.C. Cho, H. Kurz, P. Leisching, and K. Köhler, Phys. Status Solidi B **206**, 443 (1998).

[39] F. Bloch, Z. Phys. **52**, 555 (1928).

[40] G. von Plessen and P. Thomas, Phys. Rev. B **45**, 9185 (1992).

[41] T. Meier, G. von Plessen, P. Thomas, and S.W. Koch, Phys. Rev. Lett. **73**, 902 (1994).

[42] Ren-Bao Liu and Bang-Fen Zhu, Phys. Rev. B **59**, 5759 (1999).

[43] P. Leisching, W. Beck, H. Kurz, W. Schäfer, K. Leo, and K. Köhler, Phys. Rev. B **51**, 7962 (1995).

[44] K.-C. Je, Yup Kim, T. Meier, and S.W. Koch, J. Korean Phys. Soc. **32**, L437 (1998).

[45] P.H. Bolivar, F. Wolter, A. Müller, H.G. Roskos, H. Kurz, and K. Köhler, Phys. Rev. Lett. **78**, 2232 (1997).

[46] See, e.g., Claude Cohen-Tannoudji, Jacques Dupont-Roc, and Gilbert Grynberg, *Introduction to Quantum Electrodynamics* (Wiley Inter-Science, New York, 1989).

[47] M. Lindberg, R. Binder, and S.W. Koch, Phys. Rev. A **45**, 1865 (1992).

[48] P. Kner, W. Schäfer, R. Lövenich, and D.S. Chemla, Phys. Rev. Lett. **81**, 5386 (1998).

[49] Jagdeep Shah, *Ultrafast Spectroscopy of Semiconductors and Semiconductor Nanostructures* (Springer-Verlag, New York, 1996), p. 46.